
Amortized Factor Inference Networks for Posterior Inference

Joohwan Ko, Justin Domke
Manning College of Information and Computer Sciences
University of Massachusetts Amherst
{joochwanko, domke}@cs.umass.edu

Abstract

Amortized inference promises fast test-time Bayesian inference, but existing methods are inherently tied to fixed models. Extending amortization to unseen models typically requires retraining or costly test-time finetuning. In this paper, we ask: is it possible to build a single inference network capable of generalizing across varying priors, likelihoods, and dimensionality? We introduce Amortized Factor Inference Networks (AFINs), a family of encode-merge-decode inference networks built on dimension-independent modules that map a model specification and its observations to the parameters of a variational posterior. Experimentally, a single trained AFIN achieves posterior accuracy comparable to NUTS and several variational inference methods, while requiring 2 to 4 orders of magnitude less test-time compute. Code is available at <https://github.com/joochwanko/AFINs>.

1 Introduction

In amortized neural posterior estimation, one repeatedly samples (z, y) pairs from a model $p(z, y)$, and trains a predictor to map y to an approximation of $p(z|y)$. This is appealing because the cost of training is only paid once, and posterior prediction is fast at test time [40, 22, 45, 10].

Traditionally, amortization is done with a fixed model $p(z, y)$, meaning the posterior predictor must be re-trained if there is any change to the prior, likelihood, dimensionality, or number of observations. Some recent work has generalized this to consider varying numbers of observations [48, 21, 55] or varying model parameters [56]. Masked Language Inference [58] phrases posterior inference very generally as a problem of unmasking missing text in a probabilistic programming language, though accuracy is limited without model-specific finetuning. (See Section 5)

This paper asks if amortization can match the accuracy of non-amortized inference methods, while operating over an entire family of distinct Bayesian inference problems, meaning varying prior and likelihood families, varying observations, and varying dimensionality.

To achieve this, we introduce *Amortized Factor Inference Networks* (AFINs), a family of inference networks that map a model representation plus a dataset to an approximate posterior. Each AFIN has three parts: an **encoder** that maps each factor to an embedding with per-dimension and per-pair features, a **merge** that aggregates the prior and likelihood factors into a single representation, and a **decoder** that produces the final posterior parameters.

The encode-merge-decode design is inspired by conjugate Bayesian updates, in which the “embedding” would be the natural parameters and the “merge” would be addition. AFIN generalizes this view by learning a common high-dimensional representation for all factor types and using a transformer-based merge step to model interactions between factors.

To make this design applicable across varying latent dimensions, we use dimension-independent variants of MLPs and transformers. For a latent variable $z \in \mathbb{R}^d$, these modules can operate across

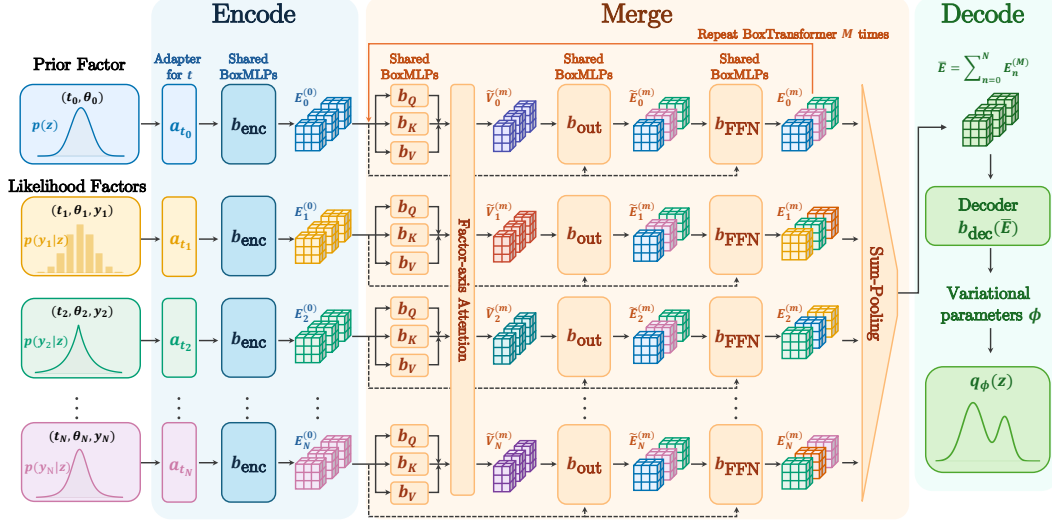


Figure 1: Architecture of an AFIN. Each factor is encoded by a type-specific adapter and shared BoxMLP, merged through M BoxTransformer blocks with factor-axis attention, sum-pooled over $n = 0, \dots, N$, and decoded into variational parameters ϕ for $q_\phi(z)$.

different values of d , have learned parameter shapes that do not depend on d , and produce outputs that are equivariant to permutations of the latent coordinates.

Experimentally, on synthetic and real problems, a single trained AFIN with roughly 5M parameters matches the performance of variational inference using full-rank Gaussians, inverse autoregressive flows [30], masked autoregressive flows [41], and neural spline flows [12], while being approximately four orders of magnitude faster. When used as a proposal for importance sampling, a trained AFIN can match or exceed the performance of NUTS [25] while being approximately two orders of magnitude faster.

2 Problem setup

We consider a family of latent-variable models whose joint density factorizes as

$$p(z, y_{1:N}) = p_0(z) \prod_{n=1}^N p_n(y_n|z), \quad (1)$$

where $z \in \mathbb{R}^d$ is the latent variable and $y_{1:N} = (y_1, \dots, y_N)$ denotes the observations. The model consists of $N + 1$ factors: one prior factor $p_0(z)$ and N likelihood factors $p_n(y_n|z)$, one for each observation.

Given a model $p(z, y_{1:N})$ and observations $y_{1:N}$, our goal is to approximate the posterior distribution $p(z|y_{1:N})$. We use a tractable variational distribution $q_\phi(z)$, whose parameters ϕ are produced by an inference network. Rather than fitting a new variational approximation for every new choice of prior, likelihood factors, and observed data, we aim to learn an amortized map from the specified factors and observations to the parameters of q_ϕ .

The factors in the model need not be homogeneous. For example, one observation may be modeled with a Gaussian likelihood, another with a Student- t likelihood, and another with a Bernoulli likelihood. Different factor families also require different factor-specific quantities: a Gaussian likelihood may use a noise scale, a Student- t likelihood may use both a scale and degrees of freedom, and a regression likelihood may include a covariate vector. These quantities may be scalars, vectors, matrices, or combinations of these.

We assume that each model is provided to the inference network in a typed-factor representation. The prior factor is represented by a type t_0 and factor-specific parameters θ_0 . Each likelihood factor is represented by a type t_n , factor-specific parameters θ_n , and observation y_n , for $n = 1, \dots, N$. Here,

“factor-specific parameters” refers to model-side quantities needed to instantiate the factor given its type, not to the learned parameters of the inference network. The type t_n determines the density family and how θ_n is interpreted, so the shape and meaning of θ_n may vary across factor types.

We assume that the possible factor types belong to a finite set. Under this typed-factor representation, the model can be written as

$$p(z, y_{1:N} \mid t_0, \theta_0, \{t_n, \theta_n\}_{n=1}^N) = p(z \mid t_0, \theta_0) \prod_{n=1}^N p(y_n \mid z, t_n, \theta_n). \quad (2)$$

Here t_0 selects the prior family and θ_0 gives its factor-specific parameters, while t_n selects the likelihood family for observation y_n and θ_n gives the corresponding factor-specific parameters.

For example, consider a model with one prior factor and three likelihood factors:

$$z \sim \mathcal{N}(0, \sigma_0^2), \quad y_1 \mid z \sim \mathcal{N}(z, \sigma_1^2), \quad (3)$$

$$y_2 \mid z \sim \text{StudentT}_{\nu_2}(z, \sigma_2), \quad y_3 \mid z \sim \text{Bernoulli}(\text{sigmoid}(x_3 z)). \quad (4)$$

Here $z, y_1, y_2 \in \mathbb{R}$, $y_3 \in \{0, 1\}$, $\nu_2 > 0$ is the degrees of freedom, and $\sigma_0, \sigma_1, \sigma_2 > 0$ and x_3 are scalar factor-specific parameters. This model can be represented by taking the factor types to be string-valued labels,

$$t_0 = \text{“gaussian prior”}, \quad t_1 = \text{“gaussian likelihood”}, \quad (5)$$

$$t_2 = \text{“student-t likelihood”}, \quad t_3 = \text{“bernoulli-logit likelihood”}, \quad (6)$$

with

$$\theta_0 = (\sigma_0), \quad \theta_1 = (\sigma_1), \quad \theta_2 = (\nu_2, \sigma_2), \quad \theta_3 = (x_3). \quad (7)$$

We now define the inference network. Given a model specification of the form in Equation (2), the network f_w , with learned parameters w , outputs the parameters ϕ of the variational distribution:

$$p(z \mid y_{1:N}) \approx q_\phi(z), \quad \phi = f_w((t_0, \theta_0), \{(t_n, \theta_n, y_n)\}_{n=1}^N). \quad (8)$$

The posterior on the left is conditioned on the fixed model specification and observations. For compactness, we sometimes write t, θ, y for the full collections of factor types, factor-specific parameters, and observations.

At a high level, f_w is trained from simulated inference problems by maximizing the conditional log density assigned to the latent draw:

$$\max_w \mathbb{E}_{t, \theta} \mathbb{E}_{p(z, y \mid t, \theta)} \left[\frac{1}{d} \log q_{f_w(t, \theta, y)}(z) \right]. \quad (9)$$

Since (z, y) is sampled from the joint model, the sampled z is an exact posterior draw after conditioning on the generated observations y . Thus, maximizing Equation (9) is equivalent, up to constants independent of w , to minimizing the expected forward KL divergence from the true posterior to the predicted variational distribution. This perspective is also useful at inference time: a forward-KL-trained approximation tends to be better suited as a proposal for importance-sampling correction. The full training and inference procedure is described in Section 4.3.

The same network with the same learned parameters w should be used across different inference problems. This creates three main challenges. First, the number of factors $N + 1$ can vary, and the likelihood factors form an unordered collection whose types may differ from one observation to another. Second, factor-specific parameters and observations can have type-dependent shapes. Third, the latent dimension d can vary, so the architecture should not have learned parameter shapes that depend on d , while its outputs should remain equivariant to permutations of the latent coordinates.

3 Dimension-Independent Building Blocks

This section describes neural network modules that can apply to varying numbers of dimensions, and where outputs are equivariant in permutations of the dimensions of the input.

3.1 BoxMLP

BoxMLP is a parameter-tied multilayer perceptron (MLP) whose learned parameter shapes are independent of the latent dimension. We introduce the construction in the simplest scalar-channel setting, where the input and output are both vectors in \mathbb{R}^d ; the same parameter-tying pattern extends to multi-channel inputs, deeper MLPs, and the node- and pair-indexed tensors used in AFIN. The implementation-level tensor versions are described in [Section B](#).

Consider a standard one-hidden-layer MLP that maps $z \in \mathbb{R}^d$ to $o \in \mathbb{R}^d$. With H hidden units, it can be written as

$$h_\ell = \sigma \left(\gamma_\ell + \sum_{i=1}^d W_{i\ell}^{\text{in}} z_i \right), \quad \ell = 1, \dots, H, \quad (10)$$

$$o_j = \delta_j + \sum_{\ell=1}^H W_{\ell j}^{\text{out}} h_\ell, \quad j = 1, \dots, d. \quad (11)$$

The input weights $W_{i\ell}^{\text{in}}$ and output weights $W_{\ell j}^{\text{out}}$ each have dH entries. The hidden biases γ_ℓ have H entries, and the output biases δ_j have d entries. Thus, for fixed hidden width H , the learned parameter shapes depend on d .

BoxMLP removes this dependence on d by tying parameters across coordinates. Instead of forming a single hidden vector $h \in \mathbb{R}^H$, it forms coordinate-wise hidden features $h_j \in \mathbb{R}^H$ as

$$h_{j\ell} = \sigma \left(\gamma_\ell + \alpha_\ell z_j + \beta_\ell \frac{1}{d} \sum_{i=1}^d z_i \right), \quad j = 1, \dots, d, \ell = 1, \dots, H, \quad (12)$$

$$o_j = \delta + \sum_{\ell=1}^H \omega_\ell h_{j\ell}, \quad j = 1, \dots, d. \quad (13)$$

Here, the coordinate-local coefficients α_ℓ , pooled-summary coefficients β_ℓ , hidden biases γ_ℓ , and output weights ω_ℓ each have H entries, while the output bias δ has one entry, meaning no parameters depend on d . It is easy to see that the output $o \in \mathbb{R}^d$ is equivariant in permutations of the input $z \in \mathbb{R}^d$. The local term $\alpha_\ell z_j$ allows o_j to depend on its own coordinate, while the mean-pooled term $\beta_\ell d^{-1} \sum_{i=1}^d z_i$ shares information across coordinates. Although we write a single pooled mean here, the same construction can use other permutation-equivariant summaries.

This scalar-channel construction is the basic pattern used throughout AFIN. In the full architecture, the local coordinate value z_j is replaced by multi-channel node or pair features, the pooled term is replaced by invariant summaries of those features, and the coordinate-wise maps can have arbitrary fixed depth and width. Consequently, changing d changes the number of coordinate-indexed evaluations, but not the learned parameter shapes.

3.2 BoxTransformer

A BoxTransformer is a dimension-independent analogue of a standard Transformer block [\[54\]](#). It keeps the usual pre-normalization pattern of input projection, self-attention, output projection, residual updates, and feed-forward refinement. The difference is that the learned maps are BoxMLPs applied to coordinate-indexed tokens, so their parameter shapes do not depend on the latent dimension d , and the resulting block is equivariant to permutations of the latent coordinates.

Consider a sequence of $N + 1$ coordinate-indexed tokens $E_{0:N} = (E_0, \dots, E_N)$, where each token has shape $E_n \in \mathbb{R}^{d \times C}$. The query, key, and value tensors are produced as

$$Q_n = b_Q(\text{LN}(E_n)), \quad K_n = b_K(\text{LN}(E_n)), \quad V_n = b_V(\text{LN}(E_n)), \quad n = 0, \dots, N. \quad (14)$$

Here b_Q, b_K, b_V are BoxMLP maps, LN denotes layer normalization, and $Q_n, K_n, V_n \in \mathbb{R}^{d \times U}$ are the query, key, and value tensors for token n , respectively, where U is the attention feature width. These are used to compute

$$\tilde{V}_{0:N} = \text{Attention}(Q_{0:N}, K_{0:N}, V_{0:N}) \in \mathbb{R}^{(N+1) \times d \times U}. \quad (15)$$

As in a standard Transformer, the attended values are projected back to the original width and added to the input through a residual connection. In BoxTransformer, this output project is implemented by a BoxMLP map b_{out} , applied in parallel over the sequence index:

$$\tilde{E}_n = E_n + b_{\text{out}} \left(\tilde{V}_n \right) \in \mathbb{R}^{d \times C}, \quad n = 0, \dots, N. \quad (16)$$

The feed-forward sublayer follows the same Transformer pattern: a normalized intermediate state is passed through a feed-forward map and added back as a residual update. Here, the feed-forward map is also a BoxMLP, applied in parallel over the sequence index:

$$E_n^+ = \tilde{E}_n + b_{\text{FFN}} \left(\text{LN} \left(\tilde{E}_n \right) \right) \in \mathbb{R}^{d \times C}, \quad n = 0, \dots, N. \quad (17)$$

Thus, the residual structure of a BoxTransformer is the standard Transformer residual structure; the dimension-independent part comes from replacing the usual dense projections and feed-forward networks with BoxMLP maps that preserve coordinate indexing. If one instead flattened each token $E_n \in \mathbb{R}^{d \times C}$ into $E_n^{\text{flat}} \in \mathbb{R}^{dC}$ and replaced $b_Q, b_K, b_V, b_{\text{out}}$, and b_{FFN} by ordinary dense projections and feed-forward networks, the same equations give a standard pre-normalization Transformer block. [Algorithm 2](#) summarizes one BoxTransformer forward pass, and [Table 5](#) makes this comparison explicit.

4 Amortized Factor Inference Networks

4.1 Motivation

Suppose that r is an exponential family with sufficient statistics T , natural parameters η and constant base measure, so that $r(z|\eta) \propto \exp(\eta^\top T(z))$. In addition, suppose that for each factor type t , there exists a function η_t such that $p(z|t, \theta) = r(z|\eta_t(\theta))$ for prior factors and $p(y|z, t, \theta) \propto r(z|\eta_t(\theta, y))$ for likelihood factors. Then, it is easy to see that the posterior would take the form

$$p(z|y_{1:N}) = r \left(z \mid \eta_{t_0}(\theta_0) + \sum_{n=1}^N \eta_{t_n}(\theta_n, y_n) \right). \quad (18)$$

This would hold in the case where the prior belongs to some exponential family that is conjugate to each of the likelihood factors. In that case, inference can be thought of as having three steps:

1. *Encoding* the prior and each of the likelihood factors (computing $\eta_{t_0}(\theta_0)$ and $\eta_{t_n}(\theta_n, y_n)$).
2. *Merging* the encoded representations (adding $\eta_{t_0}(\theta_0)$ and $\eta_{t_n}(\theta_n, y_n)$).
3. *Decoding* the merged representation (sampling / evaluating r using the merged parameters)

We want to generalize this encode-merge-decode view beyond conjugate exponential-family models. The key idea is to replace natural parameters with high-dimensional learned embeddings, use transformers to model interactions during the merge step, and to add a decoder that will map the merged embedding to a tractable variational family.

4.2 Architecture

The overall encode-merge-decode pipeline is illustrated in [Figure 1](#), and the corresponding forward pass is summarized in [Algorithm 1](#).

Encoding. AFIN first encodes each factor independently using a lightweight type-dependent adapter a_{t_n} followed by a shared encoder b_{enc} , both implemented as BoxMLPs. Let $s_0 = \theta_0$ be the prior parameters and $s_n = (\theta_n, y_n)$ the likelihood parameters for factor n . Then the embedding is

$$E_n^{(0)} = b_{\text{enc}} \left(a_{t_n} \left(s_n \right) \right), \quad n = 0, \dots, N. \quad (19)$$

In the full AFIN architecture, the coordinate-indexed embedding used in [Section 3.2](#) is extended to a node-pair embedding,

$$E_n = \left(E_n^{\text{node}}, E_n^{\text{pair}} \right), \quad E_n^{\text{node}} \in \mathbb{R}^{d \times C}, \quad E_n^{\text{pair}} \in \mathbb{R}^{d \times d \times C}. \quad (20)$$

Algorithm 1 Amortized Factor Inference Networks (AFIN). Each embedding $E_n^{(m)}$ contains a node embedding in $\mathbb{R}^{d \times C}$ and a pair embedding in $\mathbb{R}^{d \times d \times C}$.

Require: Prior factor (t_0, θ_0) , likelihood factors $\{(t_n, \theta_n, y_n)\}_{n=1}^N$
Require: Trained AFIN with learned adapters $\{a_t\}$, shared BoxMLP encoder b_{enc} , BoxTransformer blocks $\{T_m\}_{m=1}^M$, and decoder b_{dec} .

- 1: Set $s_0 \leftarrow \theta_0$ and $s_n \leftarrow (\theta_n, y_n)$ for $n = 1, \dots, N$.
- 2: **for** $n = 0, \dots, N$ **do** ▷ **Encode**; parallel over factors
- 3: $E_n^{(0)} \leftarrow b_{\text{enc}}(a_{t_n}(s_n))$ ▷ Factor-specific adapter + shared BoxMLP
- 4: **end for**
- 5: **for** $m = 1, \dots, M$ **do** ▷ **Merge**; M BoxTransformer blocks
- 6: $E_{0:N}^{(m)} \leftarrow T_m(E_{0:N}^{(m-1)})$
- 7: **end for**
- 8: $\phi \leftarrow b_{\text{dec}}\left(\sum_{n=0}^N E_n^{(M)}\right)$ ▷ pool over factor axis, then **Decode**
- 9: **return** ϕ ▷ $q_\phi(z) \approx p(z|y_{1:N})$

The node-pair representation provides a common interface for factor types with either coordinate-wise $O(d)$ parameters or pairwise $O(d^2)$ parameters, such as covariance, precision, or interaction matrices. Each factor is represented by both node and pair components with a fixed channel width C , allowing heterogeneous factor types to share an embedding space while d varies across tasks. Adapters use factor-type-specific descriptors, and BoxMLP maps are applied coordinate-wise to both d -indexed node tensors and $d \times d$ -indexed pair tensors; see [Section B.1](#) for details.

Merging. AFIN applies M BoxTransformer merge blocks to the sequence $E_{0:N}^{(0)}$, yielding updated representations $E_{0:N}^{(1)}, \dots, E_{0:N}^{(M)}$, all with the same node-pair shape. Each block extends the BoxTransformer construction to both d -indexed node features and $d \times d$ -indexed pair features, using attention across factors; see [Section B.2](#) for details. After the final merge block, AFIN sums over the factor axis to obtain a single task-level node-pair embedding, $\bar{E} = \sum_{n=0}^N E_n^{(M)}$.

Decoding. The decoder b_{dec} maps the pooled embedding to variational parameters $\phi = b_{\text{dec}}(\bar{E})$, defining an approximation $q_\phi(z) \approx p(z | y_{1:N})$. The decoder b_{dec} is again implemented as a BoxMLP trained to target a specific variational family (in our experiments, a full-rank Gaussian or normalizing flow).

Detailed adapter descriptors, merge implementation details, and decoder parameterizations are given in [Section B](#).

4.3 Training and Inference

Let f_w denote AFIN with learned parameters w . We train in a simulation-based inference setting by maximizing the log density assigned to simulator-generated latent draws:

$$\mathcal{L}(w) = \mathbb{E} \left[\frac{1}{d} \log q_{f_w(t, \theta, y)}(z) \right]. \quad (21)$$

The expectation is over a task simulator that samples the latent dimension d , number of factors N , factor types t , factor parameters θ , latent variables z , and observations y . Concretely, after sampling a model specification (d, N, t, θ) , we draw z from the prior and then draw each y_n from its likelihood conditioned on z . Equivalently, under this joint sampling procedure, the conditional distribution of the generated latent variable given the generated observations is exactly $p(z | y, t, \theta)$. Thus the sampled z can be used as a posterior draw for the simulated inference problem. The factor $1/d$ normalizes the objective across latent dimensions. The training ranges and factor families are summarized in [Section 6](#), with full details in [Section D](#).

Maximizing this objective is equivalent, up to a task-dependent constant, to minimizing the expected forward KL divergence:

$$\mathbb{E} \left[\frac{1}{d} \text{KL} (p(z | y, t, \theta) \| q_{f_w(t, \theta, y)}(z)) \right]. \quad (22)$$

Table 1: Comparison with closely related posterior inference methods. Columns indicate whether one trained inference model can handle, at test time and without retraining, changes in the number of likelihood factors N , latent dimension d , factor types t , factor-parameter shapes and values θ , and observations y . The final column summarizes whether the method is reported to reach NUTS-comparable posterior quality in its evaluated setting; it is not a controlled head-to-head comparison across all methods. \checkmark : explicit support through the test-time interface; \circ : partial support; \times : no support.

Method	vary N	vary d	vary t	vary θ	vary y	\approx NUTS
Bayesian ICL [48]	\circ	\times	\times	\times	\checkmark	\checkmark
Masked Language Inference [58]	\checkmark	\checkmark	\checkmark	\checkmark	\checkmark	\times
Masked Language Inference-Fit [58]	\times	\times	\times	\times	\checkmark	\checkmark
Simformer [21]	\circ	\times	\times	\times	\checkmark	\checkmark
Distribution Transformers [56]	\checkmark	\times	\times	\circ	\checkmark	\checkmark
NPE-PFN [55]	\circ	\circ	\times	\times	\checkmark	\checkmark
AFIN (ours)	\checkmark	\checkmark	\checkmark	\checkmark	\checkmark	\checkmark

Here the expectation is over the same simulator: first sampling d, N, t, θ , then sampling observations y from the generated model.

At inference time, we simply run [Algorithm 1](#) on a new factor specification and observations to obtain $\phi = f_w(t, \theta, y)$. The resulting q_ϕ can be used directly as a posterior approximation. When higher accuracy is desired, we also use q_ϕ as a self-normalized importance sampling (SNIS) proposal: for $z^{(s)} \sim q_\phi$, weights are proportional to the unnormalized posterior density at $z^{(s)}$ divided by $q_\phi(z^{(s)})$. This use of q_ϕ as a proposal is aligned with the forward-KL training objective: forward-KL approximations tend to be more mass-covering than reverse-KL VI approximations, which can make them better suited for importance sampling correction [38, 61, 36, 28, 17].

5 Related Work

Bayesian posterior inference is commonly handled by per-instance Monte Carlo methods such as HMC and NUTS [39, 25, 5], or by variational inference over a tractable family [4, 26, 47]. Simulation-based inference learns from simulator-generated pairs, from ABC-style methods [3, 10] to neural posterior, likelihood, and ratio estimators [40, 22, 42, 24, 13], with standard toolkits and benchmarks [52, 35]. However, these approaches typically require per-instance inference or amortization within a fixed probabilistic program, simulator, or observation interface.

Several recent methods amortize Bayesian inference over distributions of tasks. [Table 1](#) compares which variations are exposed through the test-time interface. Bayesian ICL [48] learns posterior samplers for predefined scenarios, so observations vary but d, t, θ are fixed by pretraining. Simformer [21] samples conditionals of a learned simulator joint by changing masks, but does not query inference through new typed prior-likelihood factorizations. Distribution Transformers [56] adapt GMM-represented priors, but keep the likelihood schema and latent dimension fixed. NPE-PFN [55] performs SBI from simulated parameter-observation contexts, but does not expose typed factors or arbitrary factor-parameter shapes. Masked Language Inference [58] is the closest in generality because probabilistic-program traces can represent changes in N, d, t, θ, y . However, the purely pretrained model is not reported to match NUTS-level accuracy; competitive accuracy requires per-task fitting, which we list separately as Masked Language Inference-Fit and which no longer preserves the same test-time amortization.

6 Experiments

We evaluate whether a single AFIN can perform posterior inference across changes in prior family, likelihood family, latent dimension, and number of observations. We train a roughly 5M-parameter AFIN and use the same checkpoint for all test tasks without fine-tuning (see [Table 6](#) in [Section D](#) for a module-wise breakdown). We also report AFIN+SNIS, which samples from the AFIN posterior and reweights by the unnormalized target density using the SNIS estimator in [Section 4.3](#).

AFIN is trained by maximizing $\mathcal{L}(w)$ on simulated Bayesian inference tasks. Each task samples $d \in \{1, \dots, 16\}$, $N \in \{1, \dots, 256\}$, factor types and parameters, z , and $y_{1:N}$. The generator uses

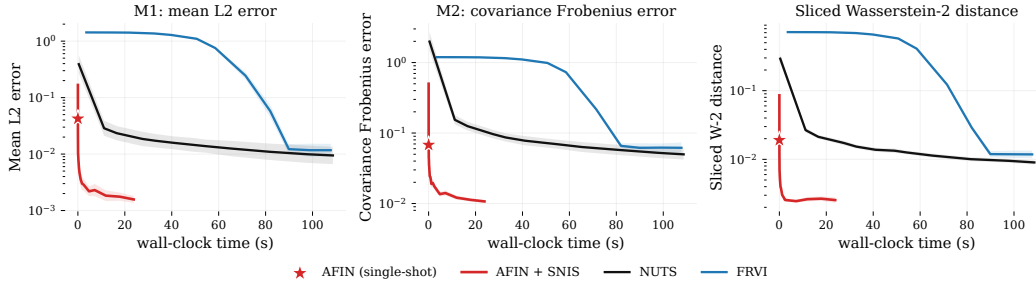


Figure 2: Synthetic posterior accuracy averaged over 16 prior-likelihood combinations and three difficulty levels. We use the Gaussian-decoder AFIN checkpoint. Points correspond to increasing test-time budgets: SNIS proposal samples for AFIN+SNIS, MCMC samples for NUTS, and optimization steps for FRVI. Posterior samples at each budget are compared with a long-run NUTS reference using mean L_2 error, covariance Frobenius error, and sliced Wasserstein-2 distance.

diagonal Gaussian, full-rank Gaussian, diagonal Laplace, and diagonal Student- t priors with Gaussian, linear Gaussian, Bernoulli-logit, binomial-logit, and linear Student- t likelihoods; likelihoods include both homogeneous and mixed-likelihood tasks. We train for 10^5 AdamW steps with cosine decay from 2×10^{-4} , batch size 32, gradient accumulation over 4 steps, and EMA weights for evaluation. Training finishes within 24 hours on a single NVIDIA H100 GPU with 80 GB of memory.

We compare against NUTS [25], full-rank Gaussian VI (FRVI), and flow-based VI baselines: inverse autoregressive flows (IAF) [30], masked autoregressive flows (MAF) [41], and neural spline flows (NSF) [12]. A long NUTS run with 10^6 iterations and 10^4 warmup iterations is used only as the posterior reference; timing plots use independent short-run NUTS chains. For VI baselines, we tune seven learning rates from 10^{-6} to 10^{-2} and report the best result at each optimization budget. For all SNIS-based curves, we evaluate proposal budgets up to 10^7 samples. We omit the amortized methods in Section 5 as direct baselines because they lack a comparable zero-shot typed-factor interface for our tasks and would require task-family-specific retraining or resimulation. As an additional posterior-predictive sanity check, Section D.8 compares a fixed trained AFIN checkpoint with TabPFN public v2 on binary OpenML classification tasks. All results use three random seeds and show mean curves with one-standard-deviation bands.

We organize the empirical evaluation into four parts. First, we study a controlled synthetic suite with 16 prior-likelihood combinations and three difficulty levels, giving 48 settings; this suite is used both to measure single-shot posterior accuracy and to evaluate AFIN as an SNIS proposal. Second, we test extrapolation beyond the training support in d , N , and both. Third, we evaluate zero-shot transfer to 12 UCI datasets, including two heterogeneous-likelihood settings. Finally, we compare Gaussian and flow decoders. See Section D for full experimental details.

6.1 Synthetic posterior inference across model families

We first evaluate one trained AFIN on a controlled synthetic suite with 16 prior-likelihood combinations and three difficulty levels: easy ($d = 4, N = 256$), medium ($d = 8, N = 64$), and hard ($d = 16, N = 1$), giving 48 settings. For each setting, AFIN receives only the typed factor specification and observations, and outputs a posterior approximation in one forward pass.

Figure 2 compares AFIN with NUTS and full-rank Gaussian VI (FRVI) using mean error, covariance error, and sliced Wasserstein-2 distance. AFIN gives a strong single-shot posterior at negligible test-time cost, and using it as an SNIS proposal further improves all metrics, reaching the accuracy of much longer NUTS and FRVI runs with substantially less wall-clock time.

6.2 AFIN as a proposal for posterior refinement

We next test AFIN as a proposal for test-time correction. We compare AFIN+SNIS with FRVI+SNIS, where FRVI proposals are obtained after 1k, 5k, or 10k optimization steps. This asks whether per-task variational optimization can produce a better SNIS proposal than the amortized AFIN posterior.

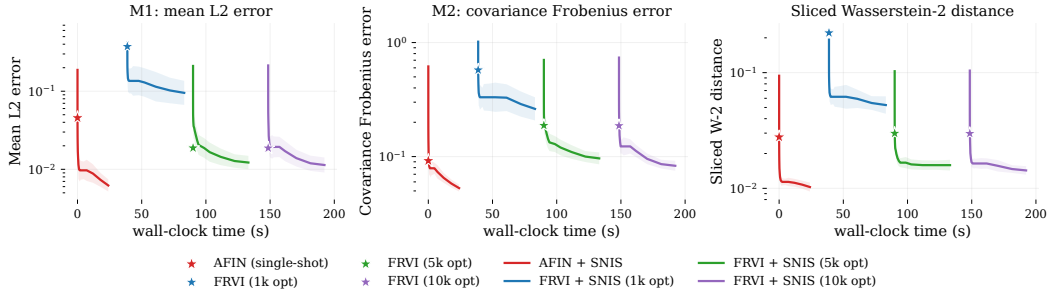


Figure 3: SNIS refinement on synthetic tasks, averaged over 16 prior–likelihood combinations and three difficulty levels. AFIN+SNIS uses the Gaussian-decoder AFIN posterior as the proposal, while FRVI+SNIS uses FRVI proposals after 1k, 5k, or 10k optimization steps. Stars denote proposal quality before SNIS; curves vary the number of SNIS proposal samples. Wall-clock time includes proposal construction, FRVI optimization when applicable, and SNIS sampling. Metrics are computed against a long-run NUTS reference.

Figure 3 shows that AFIN+SNIS improves rapidly from the single-shot posterior and is especially strong in the low-compute regime, where FRVI has not yet completed enough optimization to form an effective proposal. Even after FRVI optimization, AFIN+SNIS remains competitive across posterior mean, covariance, and sample-based metrics. To assess correction stability, Section D.6 reports Pareto- k , maximum normalized weight, entropy ratio, and target energy gap diagnostics.

6.3 Extrapolation beyond the training support

We also test whether AFIN extrapolates beyond the dimensionalities and dataset sizes seen during training. The training support is $d \leq 16$ and $N \leq 256$; we construct a small stress test that extrapolates up to $d = 32$ and $N = 512$, increasing only d , only N , or both. AFIN is evaluated zero-shot using the same checkpoint as above. AFIN+SNIS is strongest when extrapolating in N , and remains competitive on the joint d, N extrapolation while requiring less than one second of test-time computation. Pure dimension extrapolation is more challenging: short-run NUTS gives the lowest error in the OOD- d split, but at a much higher wall-clock cost. Additional metrics and experimental details are provided in Section D.7.

Table 2: Extrapolation beyond the training support. Entries report sliced Wasserstein-2 distance, mean \pm std, with wall-clock time in seconds (s) below.

Split	AFIN	AFIN+SNIS	NUTS	FRVI
OOD d	0.031 \pm .010	0.024 \pm .020	0.012\pm.006	0.042 \pm .040
	0.02s	0.24s	308s	27s
OOD N	0.027 \pm .004	0.0013\pm.0001	0.0025 \pm .0003	0.0025 \pm .0004
	0.02s	0.25s	95s	32s
OOD d, N	0.040 \pm .020	0.0039\pm.0010	0.0052 \pm .0008	0.0041 \pm .0007
	0.10s	0.45s	157s	100s

6.4 Transfer to real-world UCI tasks

We evaluate zero-shot transfer to real-world tabular datasets. We use 12 UCI tasks with regression and classification likelihoods, including two heterogeneous-likelihood settings; several tasks also involve model specifications outside the synthetic training distribution. AFIN is not fine-tuned on any UCI task; the same checkpoint trained on simulated tasks is used directly.

Figure 4 shows sliced Wasserstein-2 distance versus wall-clock time for each dataset. AFIN gives posterior approximations close to the long-run NUTS reference with almost no per-task inference cost, and AFIN+SNIS usually improves them further. Across most datasets, AFIN+SNIS reaches competitive accuracy before iterative baselines such as NUTS, FRVI, IAF VI, MAF VI, and NSF VI complete their sampling or optimization budgets. These results suggest that factor-level amortization transfers beyond the synthetic training generator to real-data posterior inference problems.

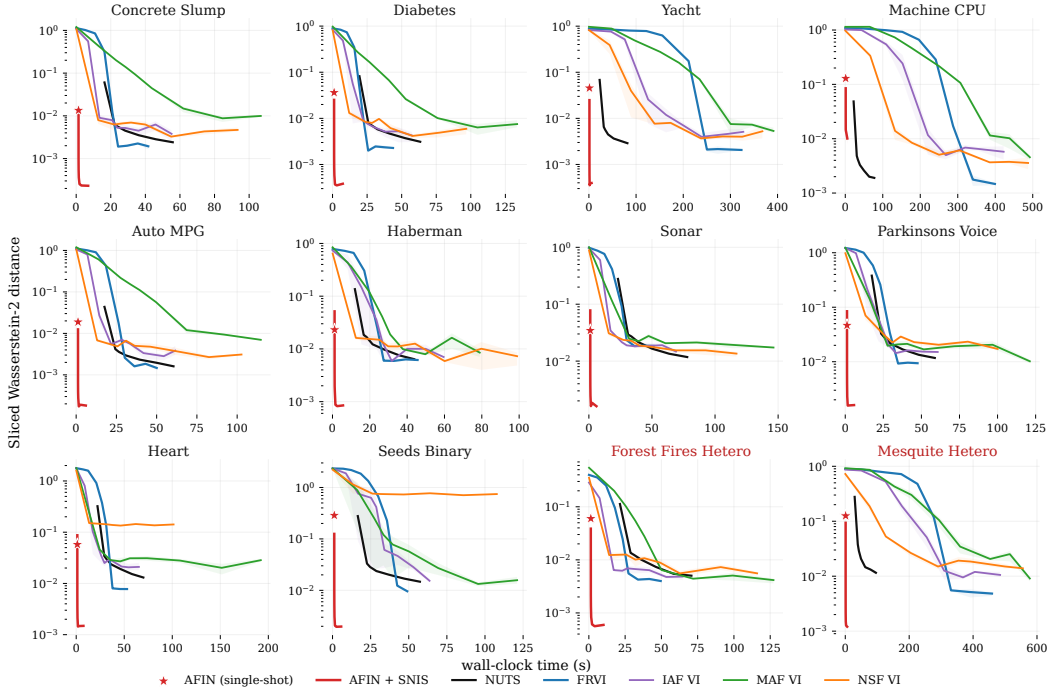


Figure 4: Zero-shot posterior inference on 12 UCI datasets using the Gaussian-decoder AFIN checkpoint. Each panel shows sliced Wasserstein-2 distance to a long-run NUTS reference versus wall-clock time. Points vary the test-time budget for AFIN+SNIS, NUTS, and VI baselines. AFIN single-shot uses one forward pass with no per-task optimization. Red titles indicate heterogeneous-likelihood tasks; shaded bands show one standard deviation over three seeds.

6.5 Gaussian versus flow decoders

Finally, we compare separately trained Gaussian- and flow-decoder AFIN variants with the same encoder-merge architecture. Table 3 shows small but consistent gains from the flow decoder, indicating that AFIN can use a more expressive variational family without changing the factor-level backbone. The decoder-only sampling time is higher for the flow because samples pass through conditional RealNVP coupling layers, but it still avoids per-task optimization and remains faster than other baselines.

Table 3: Gaussian and flow decoder variants trained with the same encoder-merge architecture. Synthetic results average over 16 prior-likelihood combinations, three difficulty levels, and three seeds; UCI results average over 12 datasets and three seeds. Lower is better for M1, M2, and W2.

Decoder	M1	M2	W2	Time (s)
<i>Synthetic</i>				
Gaussian	0.0424 \pm 0.0005	0.0679 \pm 0.0004	0.0191 \pm 0.0001	0.0087 \pm 0.0014
Flow	0.0418 \pm 0.0003	0.0671 \pm 0.0005	0.0187 \pm 0.0001	4.3521 \pm 0.0312
<i>UCI</i>				
Gaussian	0.1789 \pm 0.0012	0.1074 \pm 0.0034	0.0757 \pm 0.0023	0.0017 \pm 0.0000
Flow	0.1707 \pm 0.0010	0.1065 \pm 0.0009	0.0719 \pm 0.0008	2.7972 \pm 0.0060

7 Discussion

AFIN makes amortized Bayesian inference reusable beyond fixed models: one dimension-independent network maps typed prior and likelihood factors, together with observations, to variational posteriors across model families. Some limitations remain. AFIN assumes a predefined set of prior and likelihood factor types, so new factor families require defining descriptors and training additional adapters, although this is lightweight compared with retraining the full inference network. The current node-pair interface also does not directly represent arbitrary probabilistic-program structure, including deterministic transformations or rich hierarchical models, and its pair component scales as $O(d^2)$. Future work will extend AFIN to broader factor interfaces, richer program structure, and more scalable high-dimensional representations.

References

- [1] Abhinav Agrawal and Justin Domke. Disentangling impact of capacity, objective, batchsize, estimators, and step-size on flow vi. *International Conference on Artificial Intelligence and Statistics (AISTATS)*, 2025.
- [2] Michael Albergo, Nicholas M Boffi, and Eric Vanden-Eijnden. Stochastic interpolants: A unifying framework for flows and diffusions. *Journal of Machine Learning Research*, 2025.
- [3] Mark A Beaumont, Wenyang Zhang, and David J Balding. Approximate bayesian computation in population genetics. *Genetics*, 2002.
- [4] David M Blei, Alp Kucukelbir, and Jon D McAuliffe. Variational inference: A review for statisticians. *Journal of the American statistical Association*, 2017.
- [5] Bob Carpenter, Andrew Gelman, Matthew D. Hoffman, Daniel Lee, Ben Goodrich, Michael Betancourt, Marcus Brubaker, Jiqiang Guo, Peter Li, and Allen Riddell. Stan: A probabilistic programming language. *Journal of Statistical Software*, 2017.
- [6] Paul Edmund Chang, Nasrulloh Ratu Bagus Satrio Loka, Daolang Huang, Ulpu Remes, Samuel Kaski, and Luigi Acerbi. Amortized probabilistic conditioning for optimization, simulation and inference. In *International Conference on Artificial Intelligence and Statistics (AISTATS)*, 2025.
- [7] Małgorzata Charytanowicz, Jerzy Niewczas, Piotr Kulczycki, Piotr Kowalski, and Szymon Łukasik. Seeds. UCI Machine Learning Repository, 2010.
- [8] Hyungjin Chung, Jeongsol Kim, Michael T Mccann, Marc L Klasky, and Jong Chul Ye. Diffusion posterior sampling for general noisy inverse problems. *International Conference on Learning Representations (ICLR)*, 2023.
- [9] Paulo Cortez and Aníbal Morais. Forest Fires. UCI Machine Learning Repository, 2007.
- [10] Kyle Cranmer, Johann Brehmer, and Gilles Louppe. The frontier of simulation-based inference. *Proceedings of the National Academy of Sciences*, 2020.
- [11] Laurent Dinh, Jascha Sohl-Dickstein, and Samy Bengio. Density estimation using real nvp. In *International Conference on Learning Representations (ICLR)*, 2017.
- [12] Conor Durkan, Artur Bekasov, Iain Murray, and George Papamakarios. Neural spline flows. *Neural Information Processing Systems (NeurIPS)*, 2019.
- [13] Conor Durkan, Iain Murray, and George Papamakarios. On contrastive learning for likelihood-free inference. In *International Conference on Machine Learning (ICML)*, 2020.
- [14] Bradley Efron, Trevor Hastie, Iain Johnstone, and Robert Tibshirani. Least angle regression. *The Annals of Statistics*, 2004.
- [15] Lasse Elsemüller, Hans Olschläger, Marvin Schmitt, Paul-Christian Bürkner, Ullrich Köthe, and Stefan T. Radev. Sensitivity-aware amortized bayesian inference. *Transactions on Machine Learning Research*, 2024.
- [16] Jacob Feldmesser. Computer Hardware. UCI Machine Learning Repository, 1987.
- [17] Marylou Gabrié, Grant M. Rotskoff, and Eric Vanden-Eijnden. Adaptive monte carlo augmented with normalizing flows. *Proceedings of the National Academy of Sciences*, 2022.
- [18] Tomas Geffner, George Papamakarios, and Andriy Mnih. Compositional score modeling for simulation-based inference. In *International Conference on Machine Learning (ICML)*, 2023.
- [19] Andrew Gelman and Jennifer Hill. *Data Analysis Using Regression and Multilevel/Hierarchical Models*. Analytical Methods for Social Research. Cambridge University Press, Cambridge, 2007.
- [20] J. Gerritsma, R. Onnink, and A. Versluis. Yacht Hydrodynamics. UCI Machine Learning Repository, 1981.

- [21] Manuel Gloeckler, Michael Deistler, Christian D. Weilbach, Frank Wood, and Jakob H. Macke. All-in-one simulation-based inference. In *International Conference on Machine Learning (ICML)*, 2024.
- [22] David Greenberg, Marcel Nonnenmacher, and Jakob Macke. Automatic posterior transformation for likelihood-free inference. In *International Conference on Machine Learning (ICML)*, 2019.
- [23] S. Haberman. Haberman’s Survival. UCI Machine Learning Repository, 1976.
- [24] Joeri Hermans, Volodimir Begy, and Gilles Louppe. Likelihood-free MCMC with amortized approximate ratio estimators. In *International Conference on Machine Learning (ICML)*, 2020.
- [25] Matthew D. Hoffman and Andrew Gelman. The no-u-turn sampler: Adaptively setting path lengths in hamiltonian monte carlo. *Journal of Machine Learning Research*, 2014.
- [26] Matthew D Hoffman, David M Blei, Chong Wang, and John Paisley. Stochastic variational inference. *Journal of Machine Learning Research*, 2013.
- [27] Andras Janosi, William Steinbrunn, Matthias Pfisterer, and Robert Detrano. Heart Disease. UCI Machine Learning Repository, 1989.
- [28] Ghassen Jerfel, Serena Wang, Clara Wong-Fannjiang, Katherine A. Heller, Yian Ma, and Michael I. Jordan. Variational refinement for importance sampling using the forward kullback-leibler divergence. In *Conference on Uncertainty in Artificial Intelligence (UAI)*, 2021.
- [29] Markelle Kelly, Rachel Longjohn, and Kolby Nottingham. The UCI machine learning repository. UCI Machine Learning Repository, 2023.
- [30] Durk P Kingma, Tim Salimans, Rafal Jozefowicz, Xi Chen, Ilya Sutskever, and Max Welling. Improved variational inference with inverse autoregressive flow. In *Neural Information Processing Systems (NeurIPS)*, 2016.
- [31] Joohwan Ko and Justin Domke. Model-informed flows for bayesian inference. In *Neural Information Processing Systems (NeurIPS)*, 2025.
- [32] Tuan Anh Le, Atilim Gunes Baydin, and Frank Wood. Inference compilation and universal probabilistic programming. In *International Conference on Artificial Intelligence and Statistics (AISTATS)*, 2017.
- [33] Yaron Lipman, Ricky TQ Chen, Heli Ben-Hamu, Maximilian Nickel, and Matt Le. Flow matching for generative modeling. *International Conference on Learning Representations (ICLR)*, 2023.
- [34] Max Little. Parkinsons. UCI Machine Learning Repository, 2007.
- [35] Jan-Matthis Lueckmann, Jan Boelts, David Greenberg, Pedro Goncalves, and Jakob Macke. Benchmarking simulation-based inference. In *International Conference on Artificial Intelligence and Statistics (AISTATS)*, 2021.
- [36] Chirag Modi, Yin Li, and David Blei. Reconstructing the universe with variational self-boosted sampling. *Journal of Cosmology and Astroparticle Physics*, 2023.
- [37] Samuel Müller, Noah Hollmann, Sebastian Pineda Arango, Josif Grabocka, and Frank Hutter. Transformers can do bayesian inference. In *International Conference on Learning Representations (ICLR)*, 2022.
- [38] Christian Naesseth, Fredrik Lindsten, and David Blei. Markovian score climbing: Variational inference with $KL(p||q)$. *Neural Information Processing Systems (NeurIPS)*, 2020.
- [39] Radford M Neal. Mcmc using hamiltonian dynamics. *Handbook of markov chain monte carlo*, 2011.
- [40] George Papamakarios and Iain Murray. Fast ϵ -free inference of simulation models with bayesian conditional density estimation. In *Neural Information Processing Systems (NeurIPS)*, 2016.

- [41] George Papamakarios, Theo Pavlakou, and Iain Murray. Masked autoregressive flow for density estimation. *Neural Information Processing Systems (NeurIPS)*, 2017.
- [42] George Papamakarios, David Sterratt, and Iain Murray. Sequential neural likelihood: Fast likelihood-free inference with autoregressive flows. In *International Conference on Artificial Intelligence and Statistics (AISTATS)*, 2019.
- [43] George Papamakarios, Eric Nalisnick, Danilo Jimenez Rezende, Shakir Mohamed, and Balaji Lakshminarayanan. Normalizing flows for probabilistic modeling and inference. *Journal of Machine Learning Research*, 2021.
- [44] R. Quinlan. Auto MPG. UCI Machine Learning Repository, 1993.
- [45] Stefan T. Radev, Ulf K. Mertens, Andreas Voss, Lynton Ardizzone, and Ullrich Köthe. Bayesflow: Learning complex stochastic models with invertible neural networks. *IEEE Transactions on Neural Networks and Learning Systems*, 2022.
- [46] Stefan T. Radev, Marvin Schmitt, Valentin Pratz, Umberto Picchini, Ullrich Köthe, and Paul-Christian Bürkner. JANA: Jointly amortized neural approximation of complex bayesian models. In *Conference on Uncertainty in Artificial Intelligence (UAI)*, 2023.
- [47] Rajesh Ranganath, Sean Gerrish, and David Blei. Black Box Variational Inference. In *International Conference on Artificial Intelligence and Statistics (AISTATS)*, 2014.
- [48] Arik Reuter, Tim G. J. Rudner, Vincent Fortuin, and David Rügamer. Can transformers learn full bayesian inference in context? In *International Conference on Machine Learning (ICML)*, 2025.
- [49] Danilo Rezende and Shakir Mohamed. Variational inference with normalizing flows. In *International Conference on Machine Learning (ICML)*, 2015.
- [50] Terry Sejnowski and R. Gorman. Connectionist Bench (Sonar, Mines vs. Rocks). UCI Machine Learning Repository, 1988.
- [51] Louis Sharrock, Jack Simons, Song Liu, and Mark Beaumont. Sequential neural score estimation: Likelihood-free inference with conditional score based diffusion models. *International Conference on Machine Learning (ICML)*, 2024.
- [52] Alvaro Tejero-Cantero, Jan Boelts, Michael Deistler, Jan-Matthis Lueckmann, Conor Durkan, Pedro J. Gonçalves, David S. Greenberg, and Jakob H. Macke. sbi: A toolkit for simulation-based inference. *Journal of Open Source Software*, 2020.
- [53] Alexander Tong, Kilian Fatras, Nikolay Malkin, Guillaume Huguet, Yanlei Zhang, Jarrid Rector-Brooks, Guy Wolf, and Yoshua Bengio. Improving and generalizing flow-based generative models with minibatch optimal transport. *Transactions on Machine Learning Research*, 2024.
- [54] Ashish Vaswani, Noam Shazeer, Niki Parmar, Jakob Uszkoreit, Llion Jones, Aidan N Gomez, Łukasz Kaiser, and Illia Polosukhin. Attention is all you need. *Neural Information Processing Systems (NeurIPS)*, 2017.
- [55] Julius Vetter, Manuel Gloeckler, Daniel Gedon, and Jakob H. Macke. Effortless, simulation-efficient bayesian inference using tabular foundation models. In *Neural Information Processing Systems (NeurIPS)*, 2025.
- [56] George Whittle, Juliusz Ziomek, Jacob Rawling, and Michael A. Osborne. Distribution transformers: Fast approximate bayesian inference with on-the-fly prior adaptation, 2026.
- [57] Jonas Wildberger, Maximilian Dax, Simon Buchholz, Stephen Green, Jakob H Macke, and Bernhard Schölkopf. Flow matching for scalable simulation-based inference. *Neural Information Processing Systems (NeurIPS)*, 2023.
- [58] Mike Wu and Noah Goodman. Foundation posteriors for approximate probabilistic inference. In *Neural Information Processing Systems (NeurIPS)*, 2022.

- [59] Mike Wu, Kristy Choi, Noah D. Goodman, and Stefano Ermon. Meta-amortized variational inference and learning. In *Proceedings of the AAAI Conference on Artificial Intelligence*, 2020.
- [60] I-Cheng Yeh. Concrete Slump Test. UCI Machine Learning Repository, 2007.
- [61] Liyi Zhang, David M Blei, and Christian A Naesseth. Transport score climbing: Variational inference using forward kl and adaptive neural transport. *Transactions on Machine Learning Research*, 2023.

A Notations

Table 4 summarizes the main notation used throughout the paper. We index the prior factor by $n = 0$ and the likelihood factors by $n = 1, \dots, N$. For compactness, t, θ, y sometimes denote the full collections of factor types, factor parameters, and observations.

Table 4: Main notation used in the paper.

Symbol	Meaning
<i>Bayesian model and task specification</i>	
$z \in \mathbb{R}^d$	Latent variable; d is the latent dimension.
$y_{1:N} = (y_1, \dots, y_N)$	Observations, with one likelihood factor per observation.
N	Number of likelihood factors or observations. The full factor list has $N + 1$ factors.
$p_0(z)$	Prior factor.
$p_n(y_n z)$	n -th likelihood factor, for $n = 1, \dots, N$.
t_n	Factor type of the n -th factor. We use t_0 for the prior type.
θ_n	Parameters of factor n , valid for factor type t_n .
$s_0 = \theta_0, s_n = (\theta_n, y_n)$	Adapter inputs for the prior and likelihood factors.
<i>Inference network and posterior approximation</i>	
f_w	AFIN inference network with learned parameters w .
$\phi = f_w(t, \theta, y)$	Variational parameters output by AFIN.
$q_\phi(z)$	Variational posterior approximation to $p(z y_{1:N})$.
$\mathcal{L}(w)$	Simulation-based training objective, $\mathbb{E}[d^{-1} \log q_{f_w(t, \theta, y)}(z)]$.
<i>AFIN architecture</i>	
a_t	Type-specific adapter for factor type t .
b_{enc}	Shared BoxMLP encoder applied after the adapter.
$E_n^{(m)}$	Embedding of factor n after merge block m .
$E_n^{\text{node}} \in \mathbb{R}^{d \times C}$	Node component of a factor embedding.
$E_n^{\text{pair}} \in \mathbb{R}^{d \times d \times C}$	Pair component of a factor embedding.
C	Embedding channel width.
M	Number of BoxTransformer merge blocks.
T_m	m -th BoxTransformer merge block.
$\bar{E} = \sum_{n=0}^N E_n^{(M)}$	Task-level embedding after sum pooling over factors.
b_{dec}	Decoder mapping \bar{E} to posterior parameters ϕ .
<i>BoxMLP and BoxTransformer</i>	
H	Hidden width used in the illustrative BoxMLP definition.
U	Attention feature width in BoxTransformer.
Q_n, K_n, V_n	Query, key, and value tensors for factor n .
\tilde{V}_n	Attended value tensor for factor n .
\tilde{E}_n, E_n^+	Intermediate and output embeddings of one BoxTransformer block.
b_Q, b_K, b_V	BoxMLP maps producing queries, keys, and values.
$b_{\text{out}}, b_{\text{FFN}}$	BoxMLP output projection and feed-forward maps inside BoxTransformer.
<i>Motivation and evaluation</i>	
$r(z \eta)$	Exponential-family distribution used in the conjugate-inference motivation.
η_t	Factor-type-specific natural-parameter contribution in the conjugate case.
M1	Posterior mean error, reported as mean L_2 error.
M2	Posterior covariance error, reported as covariance Frobenius error.
W2 or SW2	Sliced Wasserstein-2 distance between approximate and reference posterior samples.
SNIS	Self-normalized importance sampling using q_ϕ as the proposal.

B Architecture Details

This appendix gives implementation-level details for the AFIN modules. The architectural motivation for BoxMLP and BoxTransformer is given in [Section 3](#); here we focus on tensor shapes and module interfaces. All learned parameter shapes are independent of the latent dimension d . Changing d only changes how many coordinate-indexed evaluations are performed.

We use plain symbols such as E , Q , K , and V for tensor-valued embeddings and attention features; their shapes are stated where they are introduced. We represent each factor by a node-pair embedding

$$E = (E^{\text{node}}, E^{\text{pair}}), \quad E^{\text{node}} \in \mathbb{R}^{d \times C}, \quad E^{\text{pair}} \in \mathbb{R}^{d \times d \times C}. \quad (23)$$

The node part stores coordinate-level information, and the pair part stores coordinate-pair information. For any pair-indexed tensor X , let

$$\text{sym}(X)_{ij} = \frac{1}{2} (X_{ij} + X_{ji}) \quad (24)$$

denote symmetrization over the two latent-coordinate indices. We apply this operation whenever a symmetric pair representation is required.

We use the shorthand

$$s_0 = \theta_0, \quad s_n = (\theta_n, y_n), \quad n = 1, \dots, N, \quad (25)$$

where the factor type t_n selects the adapter a_{t_n} . Unless otherwise stated, we use feature width $C = 40$, hidden width $H = 192$, and $L = 4$ linear layers for coordinate-wise MLPs.

Coordinate-wise maps. A coordinate-wise MLP is a map $g : \mathbb{R}^{C_{\text{in}}} \rightarrow \mathbb{R}^{C_{\text{out}}}$, implemented as an MLP with hidden width H and L linear layers, applied independently at each coordinate with shared learned weights. Thus, for $X \in \mathbb{R}^{d \times C_{\text{in}}}$,

$$[g(X)]_i = g(X_i) \in \mathbb{R}^{C_{\text{out}}}, \quad i = 1, \dots, d, \quad (26)$$

and for $X \in \mathbb{R}^{d \times d \times C_{\text{in}}}$,

$$[g(X)]_{ij} = g(X_{ij}) \in \mathbb{R}^{C_{\text{out}}}. \quad (27)$$

The same learned parameters are reused for all coordinates or coordinate pairs, so the learned parameter shapes depend on C_{in} , C_{out} , H , and L , but not on d . BoxMLP modules are built from such coordinate-wise maps after augmenting local node and pair features with invariant coordinate summaries.

B.1 Encoder

The encoder maps each raw factor specification to a common node-pair embedding. It has two stages: a factor-type-specific adapter followed by a shared BoxMLP encoder.

Inputs and factor types. The input factor specifications are $s_0 = \theta_0$ and $s_n = (\theta_n, y_n)$ for $n = 1, \dots, N$, with factor types t_0, \dots, t_N . We index factors by $n = 0, \dots, N$, where $n = 0$ denotes the prior factor.

The finite factor-type set is

$$\mathcal{T} = \mathcal{T}_{\text{prior}} \cup \mathcal{T}_{\text{like}}, \quad (28)$$

where the role of the factor is treated as part of the type. Thus, prior and likelihood factors may use different adapters even when their parametric forms are similar. In our experiments,

$$\begin{aligned} \mathcal{T}_{\text{prior}} &= \{\text{diag_gaussian}, \text{fullrank_gaussian}, \text{diag_laplace}, \text{diag_student_t}\}, \\ \mathcal{T}_{\text{like}} &= \{\text{gaussian}, \text{lin_gaussian}, \text{bernoulli_logit}, \text{binomial_logit}, \text{lin_student_t}\}. \end{aligned} \quad (29)$$

Factor-type adapters. Each factor type $t \in \mathcal{T}$ has an adapter

$$a_t = \left(a_t^{\text{node}}, a_t^{\text{pair}} \right). \quad (30)$$

The adapter converts raw factor-specific parameters, observations, and covariates into the common node-pair embedding format. Different factor types may use different descriptor widths, but all adapters return the same output shapes.

For factor n , let $t = t_n$. The raw specification s_n is converted into descriptors $\xi_{n,i}^{\text{node}} \in \mathbb{R}^{\chi_t^{\text{node}}}$ and $\xi_{n,ij}^{\text{pair}} \in \mathbb{R}^{\chi_t^{\text{pair}}}$, where χ_t^{node} and χ_t^{pair} denote the type-specific descriptor widths. The adapters are coordinate-wise MLPs

$$a_t^{\text{node}} : \mathbb{R}^{\chi_t^{\text{node}}} \rightarrow \mathbb{R}^C, \quad a_t^{\text{pair}} : \mathbb{R}^{\chi_t^{\text{pair}}} \rightarrow \mathbb{R}^C, \quad (31)$$

with hidden width H_{ad} and L_{ad} linear layers. In practice, they are smaller than the shared BoxMLP encoder because they only lift type-specific descriptors into the common embedding space. Equivalently,

$$E_n^{\text{ad}} = a_{t_n}(s_n), \quad E_n^{\text{ad}} = (E_n^{\text{node,ad}}, E_n^{\text{pair,ad}}), \quad (32)$$

where

$$E_n^{\text{node,ad}} \in \mathbb{R}^{d \times C}, \quad E_n^{\text{pair,ad}} \in \mathbb{R}^{d \times d \times C}. \quad (33)$$

The pair part is symmetrized after construction.

Example: diagonal Gaussian prior. For a diagonal Gaussian prior $z_i \sim \mathcal{N}(\mu_i, \sigma_i^2)$, we use the node descriptor

$$\xi_i^{\text{node}} = [\mu_i, \log \sigma_i, \mu_i/\sigma_i] \in \mathbb{R}^3 \quad (34)$$

and the pair descriptor

$$\xi_{ij}^{\text{pair}} = [\mu_i, \log \sigma_i, \mu_i/\sigma_i, \mu_j, \log \sigma_j, \mu_j/\sigma_j, \mathbf{1}\{i = j\}] \in \mathbb{R}^7. \quad (35)$$

Thus this factor type uses descriptor widths $\chi_{\text{diag_gaussian}}^{\text{node}} = 3$ and $\chi_{\text{diag_gaussian}}^{\text{pair}} = 7$.

Shared BoxMLP encoder. After the adapter, a shared BoxMLP encoder refines each factor independently:

$$E_n^{(0)} = b_{\text{enc}}(E_n^{\text{ad}}), \quad n = 0, \dots, N. \quad (36)$$

The same encoder parameters are used for all prior and likelihood factors.

The encoder BoxMLP refines the node and pair components by combining local features with invariant coordinate summaries. For a node-pair embedding $E = (E^{\text{node}}, E^{\text{pair}})$, define

$$\begin{aligned} \text{row}(E^{\text{pair}})_i &= \frac{1}{d} \sum_{j=1}^d E_{ij}^{\text{pair}}, & \text{col}(E^{\text{pair}})_j &= \frac{1}{d} \sum_{i=1}^d E_{ij}^{\text{pair}}, \\ \text{diag}(E^{\text{pair}})_i &= E_{ii}^{\text{pair}}, & \bar{E}^{\text{pair}} &= \frac{1}{d^2} \sum_{i,j=1}^d E_{ij}^{\text{pair}}, \\ \bar{E}^{\text{node}} &= \frac{1}{d} \sum_{i=1}^d E_i^{\text{node}}. \end{aligned} \quad (37)$$

When E^{pair} is symmetric, $\text{row}(E^{\text{pair}})_i = \text{col}(E^{\text{pair}})_i$ for each coordinate i . We keep both summaries because the same construction is reused for intermediate pair tensors that need not be symmetric.

The pair update branch receives, for each coordinate pair (i, j) , the local pair embedding together with row, column, node, and global pair summaries:

$$\xi_{ij}^{\text{pair}} = [E_{ij}^{\text{pair}}, \text{row}(E^{\text{pair}})_i, \text{col}(E^{\text{pair}})_j, E_i^{\text{node}}, E_j^{\text{node}}, \bar{E}^{\text{pair}}] \in \mathbb{R}^{6C}. \quad (38)$$

The node update branch receives, for each coordinate i , the local node embedding together with diagonal, row, column, global pair, and global node summaries:

$$\xi_i^{\text{node}} = [E_i^{\text{node}}, \text{diag}(E^{\text{pair}})_i, \text{row}(E^{\text{pair}})_i, \text{col}(E^{\text{pair}})_i, \bar{E}^{\text{pair}}, \bar{E}^{\text{node}}] \in \mathbb{R}^{6C}. \quad (39)$$

Each branch is a coordinate-wise MLP with hidden width H and L linear layers,

$$b_{\text{enc}}^{\text{node}} : \mathbb{R}^{6C} \rightarrow \mathbb{R}^C, \quad b_{\text{enc}}^{\text{pair}} : \mathbb{R}^{6C} \rightarrow \mathbb{R}^C. \quad (40)$$

Algorithm 2 BoxTransformer

Require: Sequence of $N + 1$ coordinate-indexed tokens $E_{0:N}$.

Require: BoxMLP maps $b_Q, b_K, b_V, b_{\text{out}}, b_{\text{FFN}}$; LN denotes layer normalization

- 1: Project LN($E_{0:N}$) to $Q_{0:N}, K_{0:N}, V_{0:N}$ using b_Q, b_K, b_V . ▷ Equation (14)
 - 2: Attend over the factor axis with coordinate-averaged scores to obtain $\tilde{V}_{0:N}$. ▷ Equation (15)
 - 3: Project attended values with b_{out} and add the residual to obtain $\tilde{E}_{0:N}$. ▷ Equation (16)
 - 4: Apply b_{FFN} with layer normalization and residual update to obtain $E_{0:N}^+$. ▷ Equation (17)
 - 5: **return** $E_{0:N}^+$
-

Table 5: Vanilla Transformer versus BoxTransformer for a sequence of length $N + 1$. Both compute $A \in \mathbb{R}^{(N+1) \times (N+1)}$, but only the vanilla layer uses learned maps whose shapes involve dC . The table shows the single-stream notation; the AFIN implementation uses the multi-head factor-axis version described in Section B.2.

	Vanilla Transformer	BoxTransformer
Token	$E_n^{\text{flat}} = \text{vec}(E_n) \in \mathbb{R}^{dC}$	$E_n \in \mathbb{R}^{d \times C}$
QKV	$Q_n = W_Q \text{LN}(E_n^{\text{flat}}), K_n = W_K \text{LN}(E_n^{\text{flat}}),$ $V_n = W_V \text{LN}(E_n^{\text{flat}}), Q_n, K_n, V_n \in \mathbb{R}^U$	$Q_n = b_Q(\text{LN}(E_n)), K_n = b_K(\text{LN}(E_n)),$ $V_n = b_V(\text{LN}(E_n)), Q_n, K_n, V_n \in \mathbb{R}^{d \times U}$
Score attention	$S_{n\ell} = U^{-1/2} \langle Q_n, K_\ell \rangle,$ $A_{n\ell} = \text{softmax}_\ell(S_{n\ell}), A \in \mathbb{R}^{(N+1) \times (N+1)}$	$S_{n\ell} = (d\sqrt{U})^{-1} \sum_{i=1}^d \langle Q_{n,i}, K_{\ell,i} \rangle,$ $A_{n\ell} = \text{softmax}_\ell(S_{n\ell}), A \in \mathbb{R}^{(N+1) \times (N+1)}$
Value output	$\tilde{V}_n = \sum_{\ell=0}^N A_{n\ell} V_\ell \in \mathbb{R}^U,$ $\tilde{E}_n^{\text{flat}} = E_n^{\text{flat}} + W_O \tilde{V}_n \in \mathbb{R}^{dC}$	$\tilde{V}_{n,i} = \sum_{\ell=0}^N A_{n\ell} V_{\ell,i}, \tilde{V}_n \in \mathbb{R}^{d \times U},$ $\tilde{E}_n = E_n + b_{\text{out}}(\tilde{V}_n) \in \mathbb{R}^{d \times C}$
FFN	$(E_n^{\text{flat}})^+ = \tilde{E}_n^{\text{flat}} + \text{FFN}(\text{LN}(\tilde{E}_n^{\text{flat}}))$	$E_n^+ = \tilde{E}_n + b_{\text{FFN}}(\text{LN}(\tilde{E}_n))$
Maps	$W_Q, W_K, W_V \in \mathbb{R}^{U \times dC}, W_O \in \mathbb{R}^{dC \times U}$ $\text{FFN} : \mathbb{R}^{dC} \rightarrow \mathbb{R}^{dC}$	$b_Q, b_K, b_V : \mathbb{R}^{d \times C} \rightarrow \mathbb{R}^{d \times U}$ $b_{\text{out}} : \mathbb{R}^{d \times U} \rightarrow \mathbb{R}^{d \times C}, b_{\text{FFN}} : \mathbb{R}^{d \times C} \rightarrow \mathbb{R}^{d \times C}$

The branches are applied independently at each coordinate or coordinate pair with shared weights:

$$\Delta_i^{\text{node}} = b_{\text{enc}}^{\text{node}}(\xi_i^{\text{node}}), \quad \Delta_{ij}^{\text{pair}} = b_{\text{enc}}^{\text{pair}}(\xi_{ij}^{\text{pair}}). \quad (41)$$

The encoder then applies a residual update and symmetrizes the pair state:

$$E_i^{\text{node}} \leftarrow E_i^{\text{node}} + \Delta_i^{\text{node}}, \quad E^{\text{pair}} \leftarrow \text{sym}(E^{\text{pair}} + \Delta^{\text{pair}}). \quad (42)$$

Thus $E_{ij}^{\text{pair}} = E_{ji}^{\text{pair}}$ at the end of every encoder refinement. All summaries are permutation-equivariant in the latent coordinate indices, and all learned parameter shapes depend only on $C, H,$ and L , not on d .

B.2 Merge

The merge module takes the encoded factor sequence $E_{0:N}^{(0)}$ and produces a single task-level node-pair embedding. It is implemented as a stack of M BoxTransformer blocks,

$$E_{0:N}^{(m)} = T_m(E_{0:N}^{(m-1)}), \quad m = 1, \dots, M, \quad (43)$$

followed by sum pooling over the factor axis. Thus, the learned merge operation is the BoxTransformer stack; the BoxMLP maps below are the internal projection, output, and feed-forward maps of each block. Algorithm 2 summarizes the single-block update, and Table 5 compares the corresponding factor-axis computation with a vanilla Transformer.

Each $E_n^{(m)}$ is a node-pair object,

$$E_n^{(m)} = (E_n^{\text{node},(m)}, E_n^{\text{pair},(m)}), \quad E_n^{\text{node},(m)} \in \mathbb{R}^{d \times C}, \quad E_n^{\text{pair},(m)} \in \mathbb{R}^{d \times d \times C}. \quad (44)$$

Node-pair BoxMLP maps inside a block. Every learned map inside a BoxTransformer block, $b_Q, b_K, b_V, b_{\text{out}}, b_{\text{FFN}}$, is implemented as a node-pair BoxMLP: it takes a node-pair object as input and returns a node-pair object. Each map uses separate node and pair MLP branches with the same $6C$ -dimensional summaries defined in Equations (38) and (39). The intermediate Q, K, V pair features are used to compute attention scores and values. For state updates, pair components are symmetrized after the residual update. We view b_{out} below as producing a residual increment.

Query, key, and value. At block m , layer normalization is applied before the query, key, and value maps:

$$Q_{0:N}^{(m)} = b_Q^{(m)} \left(\text{LN} \left(E_{0:N}^{(m-1)} \right) \right), \quad (45)$$

$$K_{0:N}^{(m)} = b_K^{(m)} \left(\text{LN} \left(E_{0:N}^{(m-1)} \right) \right), \quad (46)$$

$$V_{0:N}^{(m)} = b_V^{(m)} \left(\text{LN} \left(E_{0:N}^{(m-1)} \right) \right). \quad (47)$$

Each of $Q_n^{(m)}, K_n^{(m)}, V_n^{(m)}$ has node and pair components. In our implementation the attention width is $U = C$, split into h heads with per-head width $u = U/h$. The latent-coordinate axes d and $d \times d$ are not split into heads; they are contracted only when computing factor-level attention scores.

Factor-axis multi-head attention. Within each head, the attention score between factor n and factor ℓ is computed from a learned mixture of node and pair scores. Suppressing the block and head indices,

$$S_{n\ell}^{\text{node}} = \frac{1}{d} \sum_{i=1}^d \langle Q_{n,i}^{\text{node}}, K_{\ell,i}^{\text{node}} \rangle, \quad S_{n\ell}^{\text{pair}} = \frac{1}{d^2} \sum_{i=1}^d \sum_{j=1}^d \langle Q_{n,ij}^{\text{pair}}, K_{\ell,ij}^{\text{pair}} \rangle. \quad (48)$$

The factor-axis attention weights are

$$A_{n\ell} = \text{softmax}_{\ell} \left(\frac{\lambda_{\text{node}} S_{n\ell}^{\text{node}} + \lambda_{\text{pair}} S_{n\ell}^{\text{pair}}}{\sqrt{u}} \right), \quad n, \ell = 0, \dots, N, \quad (49)$$

where λ_{node} and λ_{pair} are learned scalar mixing weights shared across factor pairs and heads in the block. Within each head, the same attention matrix is used to mix node and pair values:

$$\tilde{V}_{n,i}^{\text{node}} = \sum_{\ell=0}^N A_{n\ell} V_{\ell,i}^{\text{node}}, \quad \tilde{V}_{n,ij}^{\text{pair}} = \sum_{\ell=0}^N A_{n\ell} V_{\ell,ij}^{\text{pair}}. \quad (50)$$

The outputs from all heads are concatenated along the channel dimension before the output BoxMLP is applied. Attention therefore exchanges information across factors while preserving the latent-coordinate indexing inside each factor.

Output and feed-forward updates. Let

$$\Delta_{\text{Out},0:N}^{(m)} = b_{\text{out}}^{(m)} \left(\tilde{V}_{0:N}^{(m)} \right) \quad (51)$$

be the node-pair residual increment produced by the output map. The attention output state is

$$\tilde{E}_n^{\text{node},(m)} = E_n^{\text{node},(m-1)} + \Delta_{\text{Out},n}^{\text{node},(m)}, \quad \tilde{E}_n^{\text{pair},(m)} = \text{sym} \left(E_n^{\text{pair},(m-1)} + \Delta_{\text{Out},n}^{\text{pair},(m)} \right). \quad (52)$$

The feed-forward sublayer then produces another residual increment,

$$\Delta_{\text{FFN},0:N}^{(m)} = b_{\text{FFN}}^{(m)} \left(\text{LN} \left(\tilde{E}_{0:N}^{(m)} \right) \right), \quad (53)$$

and the block output is

$$E_n^{\text{node},(m)} = \tilde{E}_n^{\text{node},(m)} + \Delta_{\text{FFN},n}^{\text{node},(m)}, \quad E_n^{\text{pair},(m)} = \text{sym} \left(\tilde{E}_n^{\text{pair},(m)} + \Delta_{\text{FFN},n}^{\text{pair},(m)} \right). \quad (54)$$

We do not use order-specific positional embeddings for likelihood factors, so the merge blocks are equivariant to permutations of the likelihood-factor order.

Pooling. After the final BoxTransformer block, AFIN pools over factors:

$$\bar{E} = \sum_{n=0}^N E_n^{(M)}. \quad (55)$$

The pair component of \bar{E} is symmetrized once more after pooling. Because pooling has no learned parameters and every BoxMLP inside the merge has parameter shapes that depend only on C , H , and L , the merge module can operate on inputs with different N and d without changing its learned parameter shapes.

B.3 Decoder

The decoder, b_{dec} , maps the pooled node-pair embedding \bar{E} to variational parameters. In our experiments, we use two decoder instantiations: a Gaussian decoder and a flow decoder. In both cases, the decoder heads are implemented with coordinate-wise MLPs or BoxMLP modules.

Gaussian decoder. For the Gaussian variational family, the decoder returns

$$\phi_G = (\mu_\phi, \Lambda_\phi), \quad q_{\phi_G}(z) = \mathcal{N}\left(z; \mu_\phi, \Lambda_\phi^{-1}\right). \quad (56)$$

Here $\mu_\phi \in \mathbb{R}^d$ and $\Lambda_\phi \in \mathbb{R}^{d \times d}$. The mean is predicted coordinate-wise from local node features, local pair features, and global node-pair summaries. The precision matrix is parameterized through symmetrized pairwise interactions, with a positive diagonal stabilization chosen to guarantee that Λ_ϕ is positive definite.

Flow decoder. For the flow-based variational family, the decoder returns data-dependent parameters for a conditional RealNVP distribution:

$$\phi_F = (c^{\text{node}}, c^{\text{pair}}, \tau, \ell), \quad (57)$$

where

$$c^{\text{node}} \in \mathbb{R}^{d \times G}, \quad c^{\text{pair}} \in \mathbb{R}^{d \times d \times G}, \quad \tau, \ell \in \mathbb{R}^d. \quad (58)$$

The context features c^{node} and c^{pair} are obtained by projecting the pooled node-pair embedding, with the pair context symmetrized over coordinate indices. The final affine shift τ and log-scale ℓ are predicted coordinate-wise from local and global node-pair summaries.

Starting from $\epsilon \sim \mathcal{N}(0, I)$, the RealNVP core applies S masked coupling layers conditioned on $(c^{\text{node}}, c^{\text{pair}})$, followed by the final affine map

$$z_i = \exp(\ell_i)v_i + \tau_i, \quad (59)$$

where v is the output of the coupling layers. Each coupling conditioner is implemented with coordinate-wise projections and a BoxMLP refinement, and its log-scale outputs are bounded for stability. The density is evaluated exactly by the change-of-variables formula. The affine and coupling heads are initialized near zero, so the flow starts near the identity map and learns non-Gaussian corrections. When a pretrained Gaussian decoder is available, the flow can optionally be applied in Gaussian-whitened coordinates, so that the identity flow recovers the Gaussian approximation.

C Extended Related Work

C.1 Recent advances in posterior inference

Recent posterior inference methods increasingly use expressive generative models as variational families, posterior samplers, or neural density estimators. Normalizing flows provide tractable invertible maps from simple base densities to flexible posteriors [49, 43], with coupling and autoregressive architectures such as RealNVP, IAF, MAF, and neural spline flows improving density evaluation, sampling, and variational approximation [11, 30, 41, 12, 1, 31]. These flow-based approximations are widely used not only in VI, but also in SBI as conditional posterior or likelihood estimators [40, 22, 42, 45]. Diffusion and score-based methods have also been adapted to posterior inference, including diffusion posterior sampling for noisy inverse problems [8] and score-based SBI methods

that learn or compose posterior scores [18, 51]. Flow-matching methods further train continuous normalizing flows through vector-field regression [33, 53, 2], and have recently been applied to scalable SBI [57]. These works show that flow-, diffusion-, and flow-matching models are powerful posterior approximators, but they typically operate within a fixed model, simulator, or task interface rather than a single typed factor interface shared across varying N, d, t, θ, y .

C.2 Additional task-amortized and program-based inference

Several methods amortize inference for simulator-defined model families. BayesFlow learns globally amortized posterior estimators using invertible neural networks and learned summaries for a fixed simulator family [45]. JANA extends this direction by jointly amortizing posterior and likelihood approximations, enabling additional quantities such as marginal likelihoods and posterior predictive estimates [46]. SA-ABI uses weight sharing to support sensitivity analysis over alternative prior, likelihood, and data choices in simulation-based inference [15]. These methods reduce repeated inference cost, but their amortization is organized around simulator families or sensitivity variants rather than explicit heterogeneous Bayesian factor specifications.

Other work studies broader pretrained or program-based inference interfaces. PFNs learn Bayesian posterior prediction over supervised tasks sampled from a task prior, but they target predictive distributions rather than explicit latent posteriors [37]. ACE provides a general amortized conditioning engine over data and latent-variable tokens, allowing runtime conditioning on observed data, interpretable latents, and priors [6]. Inference Compilation trains neural proposal distributions for probabilistic programs and uses them inside sequential importance sampling [32]. Meta-amortized VI shares inference computation across related generative models [59]. These methods broaden the scope of amortized inference, but they do not expose the posterior inference problem as a typed factor list with dimension-independent posterior decoding.

D Experiment Details

This section gives additional implementation and evaluation details for the experiments in Section 6. Training runs use a single NVIDIA H100 GPU with 80 GB of memory, and evaluation runs use a single NVIDIA A100 GPU with 80 GB of memory.

D.1 Model configuration

Table 6 reports the module-wise parameter count for the default AFIN configuration. The model uses feature width $C = 40$, BoxMLP and merge hidden width $H = 192$, BoxMLP encoder depth 4, and $M = 4$ BoxTransformer merge blocks. The flow decoder uses $S = 4$ RealNVP coupling layers with hidden width 32.

The factor-type adapters, shared BoxMLP encoder, and BoxTransformer merge stack form a common backbone reused across decoder variants. Each BoxMLP-style node-pair map has separate coordinate-wise MLP heads for the node component E^{node} and pair component E^{pair} . Thus, a node-pair map with a $6C$ -dimensional input summary and C -dimensional output has roughly twice the parameters of a single $6C \rightarrow C$ coordinate-wise MLP. The same accounting applies to the $Q/K/V/Out$ maps and the feed-forward map inside each BoxTransformer block.

The Gaussian and flow decoders are trained as separate posterior heads. The Gaussian head outputs the mean and precision of a full-rank Gaussian. For the flow variant, the Gaussian decoder is kept fixed and the trainable flow-specific components are the context projection, final affine map, and RealNVP coupling layers; see Section B.3. This gives 4.55 M trainable parameters for the Gaussian variant and 5.05 M for the flow variant.

All learned maps are coordinate-wise MLPs, BoxMLP heads, or BoxTransformer blocks whose parameter shapes do not depend on d or N . Changing d or N changes only the number of coordinate- or factor-indexed evaluations, not the learned parameter shapes.

Table 6: Module-wise parameter counts for the default AFIN configuration. Counts are independent of the latent dimension d and the number of likelihood factors N . The Gaussian and flow posterior heads are trained as separate variants.

Module	# parameters
<i>Shared backbone</i>	
Factor-type adapters	55,376
BoxMLP encoder	728,384
BoxTransformer merge stack ($M = 4$)	3,643,208
<i>Gaussian posterior head</i>	
Gaussian decoder	123,043
<i>Flow posterior head</i>	
Flow context projection	128,960
Flow final affine	80,802
RealNVP flow ($S = 4$)	414,728
Trainable parameters, Gaussian posterior	4,550,011
Trainable parameters, flow posterior	5,051,458

D.2 Data-generating process

This section describes the simulator used to train AFIN. At every gradient step, we generate a fresh batch of Bayesian inference tasks; no training example is reused. The training distribution is therefore fully specified by the sampling procedure below.

Micro-batch structure. Each optimizer step uses K micro-batches of B tasks. Tasks within a micro-batch share the same latent dimension d and number of likelihood factors N , which allows efficient batching, but all other quantities are sampled independently across tasks. These include prior type, likelihood types, factor parameters, covariates, latent variables, and observations. We use $B = 32$ and $K = 4$, so each optimizer step contains 128 independent tasks.

Sampling task sizes. We sample (d, N) from a mixture of a uniform distribution and a hard-biased distribution. With probability $p_{\text{hard}} = 0.6$, (d, N) is drawn from

$$\mathbb{P}(d, N) \propto \left(\frac{d - d_{\min} + 1}{d_{\max} - d_{\min} + 1} \right)^{\alpha_d} \left(\frac{N_{\min}}{N} \right)^{\alpha_N}, \quad \alpha_d = 1.0, \quad \alpha_N = 0.75. \quad (60)$$

Otherwise, (d, N) is drawn uniformly from $\{d_{\min}, \dots, d_{\max}\} \times \{N_{\min}, \dots, N_{\max}\}$. This bias increases the frequency of high-dimensional, data-poor tasks, which are empirically harder under uniform sampling. We use

$$d_{\min} = 1, \quad d_{\max} = 16, \quad N_{\min} = 1, \quad N_{\max} = 256.$$

Sampling the prior factor. For each task, we sample the prior type uniformly from

$$\mathcal{T}_{\text{prior}} = \{\text{diag_gaussian}, \text{fullrank_gaussian}, \text{diag_student_t}, \text{diag_laplace}\}.$$

The prior location is sampled as $\mu \sim 0.45 \mathcal{N}(0, I_d)$. Type-specific dispersion parameters are sampled as follows:

- **diag_gaussian:** $\log \sigma_i \sim \text{Uniform}(-0.8, 0)$;
- **fullrank_gaussian:** precision $\Lambda = MM^\top/d + 0.5I_d$, with $M \sim 0.3 \mathcal{N}(0, I_{d \times d})$;
- **diag_student_t:** $\log \sigma_i \sim \text{Uniform}(-0.7, 0)$ and $\nu \sim \text{Uniform}(3, 8)$;
- **diag_laplace:** $\log s_i \sim \text{Uniform}(-1.0, -0.05)$.

We then sample z from the resulting prior.

Sampling likelihood factor types. Likelihood types are drawn from

$$\mathcal{T}_{\text{like}} = \{\text{gaussian}, \text{lin_gaussian}, \text{bernoulli_logit}, \text{binomial_logit}, \text{lin_student_t}\}.$$

With probability 0.5, the task is homogeneous: all N likelihood factors share one type drawn uniformly from $\mathcal{T}_{\text{like}}$. Otherwise, we sample a heterogeneous task. We first draw the number of distinct likelihood types

$$k \in \{2, \dots, \min(|\mathcal{T}_{\text{like}}|, N)\}, \quad \mathbb{P}(k) \propto \exp(-(k-2)),$$

choose k types uniformly without replacement, and sample mixture weights $\pi \sim \text{Dirichlet}(0.5 \mathbf{1}_k)$. We allocate the remaining $N - k$ sites with a multinomial draw using π , include at least one site of each selected type, and randomly permute the resulting list across likelihood indices.

Sampling covariates. For likelihoods with linear predictors, we sample a design matrix $X \in \mathbb{R}^{N \times d}$. Conditional on the task, the design family is drawn from

$$\{\text{iid}, \text{diag_scale}, \text{correlated}, \text{student_t}\}$$

with probabilities (0.7, 0.1, 0.1, 0.1). The base scale is $0.9/\sqrt{d}$, so the linear signal Xz remains $O(1)$. The design families are:

- **iid**: rows are isotropic Gaussian;
- **diag_scale**: rows are Gaussian with a sampled diagonal spectrum;
- **correlated**: rows are Gaussian with a sampled spectrum and random orthogonal rotation;
- **student_t**: as in **correlated**, with row-wise multiplicative weights giving multivariate Student- t tails.

Sampling observations. Given z and any required covariates, each likelihood factor samples its observation from the corresponding density. For **lin_gaussian** and **lin_student_t**,

$$y_n = x_n^\top z + \varepsilon_n,$$

with Gaussian or Student- t noise and sampled scale parameters. For **bernoulli_logit**,

$$y_n \sim \text{Bernoulli}(\sigma(x_n^\top z)),$$

and for **binomial_logit**, we sample $n_c \sim \text{Uniform}\{2, \dots, 8\}$ and then

$$y_n \sim \text{Binomial}(n_c, \sigma(x_n^\top z)).$$

For the non-regression **gaussian** likelihood, we sample a vector observation $y_n \in \mathbb{R}^d$ as

$$y_n = z + \varepsilon_n,$$

with sampled isotropic Gaussian noise. In this case, the network receives a per-site descriptor built from y_n rather than from a covariate row.

Simulator output. The simulator returns the factor specification and observations,

$$(t_0, \theta_0, \{(t_n, \theta_n, y_n)\}_{n=1}^N),$$

together with the latent draw z . The factor specification and observations are the input to AFIN, while z is the target used in the training objective $\mathcal{L}(w)$. Since each task is generated by first drawing z from the prior and then drawing observations from the likelihoods, the sampled z is an exact posterior draw conditioned on the simulated observations. This defines the task distribution over d, N , factor types, parameter shapes, covariates, and observation regimes used to train AFIN.

D.3 Evaluation metrics

We evaluate approximate posteriors against a long-run NUTS reference. For a fixed task and fixed observations $y_{1:N}$, let

$$\tilde{p}_y(z) = p(z, y_{1:N})$$

denote the unnormalized posterior density. Let

$$z_q^{(1)}, \dots, z_q^{(S)} \sim q_\phi(z), \quad z_{\text{ref}}^{(1)}, \dots, z_{\text{ref}}^{(S_{\text{ref}})} \sim p_{\text{ref}}(z \mid y_{1:N})$$

denote samples from an approximate posterior and from the NUTS reference, respectively. For unweighted samples, we define

$$\hat{\mu}_q = \frac{1}{S} \sum_{s=1}^S z_q^{(s)}, \quad \hat{\Sigma}_q = \frac{1}{S-1} \sum_{s=1}^S \left(z_q^{(s)} - \hat{\mu}_q \right) \left(z_q^{(s)} - \hat{\mu}_q \right)^\top,$$

with $\hat{\mu}_{\text{ref}}$ and $\hat{\Sigma}_{\text{ref}}$ defined analogously from the reference samples.

Posterior mean error. We report mean accuracy using the Euclidean distance between empirical posterior means:

$$\text{M1} = \|\hat{\mu}_q - \hat{\mu}_{\text{ref}}\|_2. \quad (61)$$

Posterior covariance error. We report covariance accuracy using the Frobenius distance between empirical covariance matrices:

$$\text{M2} = \left\| \hat{\Sigma}_q - \hat{\Sigma}_{\text{ref}} \right\|_F. \quad (62)$$

Sliced Wasserstein-2 distance. We also compare the full sample distributions with sliced Wasserstein-2 distance. Let $\theta_1, \dots, \theta_R$ be random unit directions in \mathbb{R}^d . For direction θ_r , let

$$a_{r,(1)} \leq \dots \leq a_{r,(S)} \quad \text{and} \quad b_{r,(1)} \leq \dots \leq b_{r,(S)}$$

be the sorted projections $\{\theta_r^\top z_q^{(s)}\}_{s=1}^S$ and $\{\theta_r^\top z_{\text{ref}}^{(s)}\}_{s=1}^S$, using the same number of samples from each distribution. We estimate

$$\text{SW}_2 = \left[\frac{1}{R} \sum_{r=1}^R \frac{1}{S} \sum_{s=1}^S (a_{r,(s)} - b_{r,(s)})^2 \right]^{1/2}. \quad (63)$$

We use $R = 128$ random projections. For SNIS-corrected samples, we compute the same quantity using the corresponding weighted one-dimensional empirical distributions.

Self-normalized importance sampling. For AFIN+SNIS and FRVI+SNIS, we draw proposal samples $z_q^{(s)} \sim q_\phi$ and compute

$$w_s = \frac{\tilde{p}_y(z_q^{(s)})}{q_\phi(z_q^{(s)})}, \quad \bar{w}_s = \frac{w_s}{\sum_{j=1}^S w_j}. \quad (64)$$

The SNIS approximation is the weighted empirical measure

$$\hat{p}_{\text{SNIS}} = \sum_{s=1}^S \bar{w}_s \delta_{z_q^{(s)}}. \quad (65)$$

For M1 and M2, we use the weighted mean and covariance

$$\hat{\mu}_{\text{SNIS}} = \sum_{s=1}^S \bar{w}_s z_q^{(s)}, \quad (66)$$

$$\hat{\Sigma}_{\text{SNIS}} = \sum_{s=1}^S \bar{w}_s \left(z_q^{(s)} - \hat{\mu}_{\text{SNIS}} \right) \left(z_q^{(s)} - \hat{\mu}_{\text{SNIS}} \right)^\top. \quad (67)$$

SNIS diagnostics. To assess importance-weight stability, we report several diagnostics. The PSIS Pareto- k statistic is obtained by fitting a generalized Pareto distribution to the upper tail of the raw importance ratios:

$$\hat{k}_{\text{PSIS}} = \text{GPDSshape}(\text{tail}\{w_s\}_{s=1}^S). \quad (68)$$

Smaller values indicate more stable weights; as a common rule of thumb, $\widehat{k}_{\text{PSIS}} < 0.5$ indicates reliable weights, $0.5 \leq \widehat{k}_{\text{PSIS}} < 0.7$ is often usable, and larger values suggest instability.

We also report the maximum normalized weight,

$$w_{\max} = \max_{s=1, \dots, S} \bar{w}_s, \quad (69)$$

where large values indicate that a few samples dominate the estimate. The entropy ratio of the normalized weights is

$$H_{\text{ratio}} = \frac{-\sum_{s=1}^S \bar{w}_s \log \bar{w}_s}{\log S}, \quad (70)$$

which lies in $[0, 1]$, with values near 1 indicating diffuse weights.

Finally, we report a target energy gap, which measures whether approximate samples lie in regions of similar unnormalized posterior density as the reference samples. For an unweighted approximation,

$$\Delta E = \frac{1}{S} \sum_{s=1}^S \left[-\log \tilde{p}_y(z_q^{(s)}) \right] - \frac{1}{S_{\text{ref}}} \sum_{s=1}^{S_{\text{ref}}} \left[-\log \tilde{p}_y(z_{\text{ref}}^{(s)}) \right]. \quad (71)$$

For SNIS-corrected samples, the first expectation is weighted:

$$\Delta E_{\text{SNIS}} = \sum_{s=1}^S \bar{w}_s \left[-\log \tilde{p}_y(z_q^{(s)}) \right] - \frac{1}{S_{\text{ref}}} \sum_{s=1}^{S_{\text{ref}}} \left[-\log \tilde{p}_y(z_{\text{ref}}^{(s)}) \right]. \quad (72)$$

Values close to zero indicate that the approximation places mass in regions with similar target density to the NUTS reference.

D.4 Synthetic evaluation tasks

The main synthetic evaluation suite tests zero-shot posterior inference across changes in prior family, likelihood family, latent dimension, and number of observations. We evaluate all 4×4 prior-likelihood combinations. The prior families are diagonal Gaussian, full-rank Gaussian, diagonal Laplace, and diagonal Student- t . The likelihood families are linear Gaussian, Bernoulli-logit, binomial-logit, and linear Student- t , giving 16 combinations in total.

Table 7: Synthetic evaluation difficulty levels.

Difficulty	Latent dimension d	Number of observations N
Easy	4	256
Medium	8	64
Hard	16	1

For each prior-likelihood combination, we evaluate three difficulty levels. This gives $16 \times 3 = 48$ synthetic settings. The easy setting is low-dimensional and data-rich, while the hard setting is high-dimensional and data-poor. For each setting, we generate three independent random seeds. AFIN is evaluated zero-shot: it receives only the typed factor specification, factor parameters, and observations, and no synthetic evaluation task is used for fine-tuning.

Reference posterior samples are obtained with a long NumPyro NUTS run using 10^6 post-warmup samples and 10^4 warmup steps. We compare AFIN single-shot, AFIN+SNIS, short-run NUTS, and full-rank Gaussian VI (FRVI). AFIN single-shot draws samples from the Gaussian posterior produced by one forward pass. AFIN+SNIS uses this posterior as an importance proposal and reweights samples by the unnormalized target density. Short-run NUTS curves use independent chains with increasing post-warmup sample budgets. FRVI is optimized separately for each task using the learning-rate tuning protocol described in Section 6, and is evaluated at increasing optimization budgets. All methods are compared to the long-run NUTS reference using the metrics in Section D.3: posterior mean error, posterior covariance error, and sliced Wasserstein-2 distance.

We also use the same 48-setting suite to evaluate proposal quality for SNIS refinement. In this experiment, AFIN+SNIS is compared with FRVI+SNIS, where the FRVI proposals are obtained after 1k, 5k, or 10k optimization steps. This isolates whether the amortized AFIN posterior is already an effective importance proposal before task-specific optimization.

D.5 Real-world UCI tasks

We evaluate zero-shot transfer on 12 real-world tabular datasets derived from UCI-style benchmarks [29]. Each dataset is converted to the same typed-factor interface used by AFIN: one prior factor over z and one likelihood factor per observation. Continuous covariates are standardized and represented through a whitened design matrix; regression targets are standardized when appropriate. The same trained AFIN checkpoint is used for all datasets without fine-tuning.

Table 8: Real-world task specifications. Dataset sources are cited in the caption. [60, 14, 20, 16, 44, 23, 50, 34, 27, 7, 9, 19]

Dataset	d	N	Prior family	Likelihood family
Concrete Slump	7	103	Diagonal Laplace	Linear Gaussian
Diabetes	10	442	Diagonal Laplace	Linear Gaussian
Yacht	6	308	Diagonal Gaussian	Linear Student- t
Machine CPU	6	209	Diagonal Laplace	Linear Gaussian
Auto MPG	7	392	Diagonal Laplace	Linear Gaussian
Haberman	3	306	Diagonal Gaussian	Bernoulli-logit
Sonar top-8	8	208	Diagonal Student- t	Bernoulli-logit
Parkinsons Voice top-8	8	195	Diagonal Gaussian	Bernoulli-logit
Heart	13	297	Diagonal Gaussian	Bernoulli-logit
Seeds Binary	7	210	Diagonal Gaussian	Bernoulli-logit
Forest Fires Hetero	8	517	Diagonal Student- t	Heterogeneous
Mesquite Hetero	7	46	Diagonal Gaussian	Heterogeneous

The regression tasks use Gaussian or Student- t likelihoods, and the binary classification tasks use Bernoulli-logit likelihoods. Several datasets have $N > 256$, which are outside the synthetic training distribution.

For the two heterogeneous tasks, we start from an underlying regression dataset and convert half of the observations into binary threshold observations. In Forest Fires Hetero, the continuous response is, $\log(1 + \text{area})$, modeled with a Student- t likelihood, while the remaining observations are binary labels indicating whether burned area is above the dataset median, modeled with a Bernoulli-logit likelihood. In Mesquite Hetero, the continuous observations are mesquite biomass measurements, modeled with a Gaussian likelihood, while the remaining observations are binary above-median biomass labels, again modeled with a Bernoulli-logit likelihood. Thus, both tasks share one latent regression coefficient vector z , but different observations expose different aspects of the same response: some provide real-valued measurements and others provide coarsened threshold information. This is represented as a heterogeneous factorization because each row contributes its own likelihood factor $p_n(y_n | z, t_n, \theta_n)$, with t_n varying across observations.

For each dataset, we evaluate three random seeds. The reference posterior is computed with a long NumPyro NUTS run using 10^6 post-warmup samples and 10^4 warmup steps. We compare AFIN, AFIN+SNIS, short-run NUTS, FRVI, IAF VI, MAF VI, and NSF VI. Variational baselines are optimized separately for each task and evaluated along their optimization trajectories. The real-world curves report sliced Wasserstein-2 distance to the long-run NUTS reference as a function of test-time wall-clock cost.

D.6 SNIS stability diagnostics

Since AFIN+SNIS uses the amortized posterior as an importance proposal, posterior accuracy depends on both sample quality and weight stability. We therefore report diagnostics for the normalized SNIS weights \bar{w}_s : Pareto- k , maximum normalized weight, entropy ratio, and target energy gap, all defined in Section D.3. Lower Pareto- k and maximum weight indicate less tail instability and less weight concentration; higher entropy ratio indicates more diffuse weights; and energy gaps closer to zero indicate that corrected samples lie in target-density regions similar to the NUTS reference.

Table 9 reports these diagnostics by difficulty level and overall. AFIN+SNIS has stable weights across the synthetic suite without per-task optimization. On medium tasks, FRVI+SNIS after 1k optimization steps shows clear weight concentration, with large maximum weight, low entropy ratio, and a positive energy gap, while AFIN+SNIS is already comparable to FRVI+SNIS after 5k or 10k

Table 9: SNIS weight-stability diagnostics on the synthetic evaluation suite. Entries report mean \pm standard deviation. Lower is better for Pareto- k and maximum normalized weight; higher is better for entropy ratio; energy gap is best near zero. Energy gap is computed as the difference in expected negative unnormalized log posterior between the SNIS approximation and the long-run NUTS reference.

Split	Method	Pareto- k	Max weight	Entropy ratio	Energy gap
Easy	AFIN+SNIS	0.116 \pm 0.014	7.24 $\times 10^{-7}$ _{$\pm 1.2 \times 10^{-7}$}	0.998 \pm 0.000	-0.001 \pm 0.000
	FRVI+SNIS (1k)	-0.392 \pm 0.007	7.18 $\times 10^{-6}$ _{$\pm 2.8 \times 10^{-7}$}	0.902 \pm 0.000	-0.002 \pm 0.001
	FRVI+SNIS (5k)	0.153 \pm 0.013	1.62 $\times 10^{-6}$ _{$\pm 5.8 \times 10^{-7}$}	1.000 \pm 0.000	-0.002 \pm 0.000
	FRVI+SNIS (10k)	0.160 \pm 0.023	1.48 $\times 10^{-6}$ _{$\pm 7.0 \times 10^{-7}$}	1.000 \pm 0.000	-0.002 \pm 0.000
Medium	AFIN+SNIS	0.261 \pm 0.010	2.04 $\times 10^{-5}$ _{$\pm 1.3 \times 10^{-5}$}	0.997 \pm 0.000	-0.002 \pm 0.001
	FRVI+SNIS (1k)	0.558 \pm 0.018	8.05 $\times 10^{-2}$ _{$\pm 3.0 \times 10^{-2}$}	0.812 \pm 0.012	0.401 \pm 0.154
	FRVI+SNIS (5k)	0.268 \pm 0.014	2.17 $\times 10^{-5}$ _{$\pm 1.2 \times 10^{-5}$}	0.998 \pm 0.000	-0.002 \pm 0.001
	FRVI+SNIS (10k)	0.266 \pm 0.016	2.01 $\times 10^{-5}$ _{$\pm 7.7 \times 10^{-6}$}	0.998 \pm 0.000	-0.002 \pm 0.001
Hard	AFIN+SNIS	0.418 \pm 0.014	1.93 $\times 10^{-3}$ _{$\pm 1.2 \times 10^{-3}$}	0.968 \pm 0.001	-0.036 \pm 0.010
	FRVI+SNIS (1k)	0.560 \pm 0.016	1.52 $\times 10^{-2}$ _{$\pm 1.7 \times 10^{-2}$}	0.929 \pm 0.013	0.031 \pm 0.220
	FRVI+SNIS (5k)	0.465 \pm 0.020	4.38 $\times 10^{-3}$ _{$\pm 4.0 \times 10^{-3}$}	0.965 \pm 0.005	-0.079 \pm 0.030
	FRVI+SNIS (10k)	0.463 \pm 0.018	4.53 $\times 10^{-3}$ _{$\pm 3.6 \times 10^{-3}$}	0.966 \pm 0.003	-0.073 \pm 0.037
Overall	AFIN+SNIS	0.265 \pm 0.013	6.51 $\times 10^{-4}$ _{$\pm 4.0 \times 10^{-4}$}	0.988 \pm 0.000	-0.013 \pm 0.004
	FRVI+SNIS (1k)	0.242 \pm 0.014	3.19 $\times 10^{-2}$ _{$\pm 1.5 \times 10^{-2}$}	0.881 \pm 0.008	0.144 \pm 0.125
	FRVI+SNIS (5k)	0.295 \pm 0.016	1.47 $\times 10^{-3}$ _{$\pm 1.4 \times 10^{-3}$}	0.988 \pm 0.002	-0.028 \pm 0.011
	FRVI+SNIS (10k)	0.296 \pm 0.019	1.52 $\times 10^{-3}$ _{$\pm 1.2 \times 10^{-3}$}	0.988 \pm 0.001	-0.026 \pm 0.013

Table 10: Extrapolation results for posterior mean error. Entries report mean L_2 error, mean \pm standard deviation over six runs, with mean wall-clock time in parentheses. Bold indicates the lowest error in each split.

Split	AFIN	AFIN+SNIS	NUTS	FRVI
OOD d	0.134 \pm 0.044 (0.02s)	0.068 \pm 0.063 (0.24s)	0.0277 \pm 0.019 (308s)	0.0872 \pm 0.074 (27s)
OOD N	0.0799 \pm 0.011 (0.02s)	0.00185 \pm 0.0006 (0.25s)	0.00248 \pm 0.0008 (95s)	0.00603 \pm 0.002 (32s)
OOD d, N	0.205 \pm 0.103 (0.10s)	0.00984 \pm 0.005 (0.45s)	0.0110 \pm 0.004 (157s)	0.0143 \pm 0.003 (100s)

optimization steps. On hard tasks, all proposals are more challenging, but AFIN+SNIS remains in a usable Pareto- k regime and has lower maximum weight than early FRVI+SNIS. Overall, the correction is not dominated by a small number of high-weight samples, and the amortized AFIN posterior is competitive with FRVI proposals obtained after substantial per-task optimization.

D.7 Extrapolation beyond the training support

We evaluate whether AFIN extrapolates beyond the synthetic training support, where training tasks satisfy $d \leq 16$ and $N \leq 256$. We construct six out-of-support synthetic tasks, grouped into three splits: OOD d , OOD N , and OOD d, N . The OOD- d split uses $(d, N) = (24, 128)$ and $(32, 64)$; the OOD- N split uses $(12, 400)$ and $(8, 512)$; and the OOD- d, N split uses $(24, 384)$ and $(32, 400)$. Each (d, N) configuration is evaluated with three random seeds, giving six runs per split.

Reference metrics are computed from a long NumPyro NUTS run with 10^6 post-warmup samples and 10^4 warmup steps. We compare AFIN single-shot with 5×10^4 posterior samples, AFIN+SNIS with 5×10^4 proposal samples, short-run NUTS with 5×10^4 samples after 10^3 warmup steps, and FRVI optimized for 10^4 steps. For FRVI, we tune over seven logarithmically spaced learning rates from 10^{-6} to 10^{-2} , select the best result, and draw 5×10^4 samples from the optimized variational posterior. All entries report mean \pm standard deviation over the six runs in each split, with mean per-task wall-clock time in parentheses.

AFIN single-shot remains fast in all extrapolation settings, but the largest gains come from using AFIN as an SNIS proposal. AFIN+SNIS is competitive with short-run NUTS and FRVI on OOD N and OOD d, N while requiring less than one second of test-time computation. OOD d is the

Table 11: Extrapolation results for posterior covariance error. Entries report covariance Frobenius error, mean \pm standard deviation over six runs, with mean wall-clock time in parentheses. Bold indicates the lowest error in each split.

Split	AFIN	AFIN+SNIS	NUTS	FRVI
OOD d	0.234 \pm 0.164 (0.02s)	0.323 \pm 0.307 (0.24s)	0.131 \pm 0.105 (308s)	0.384 \pm 0.356 (27s)
OOD N	0.00580 \pm 0.0023 (0.02s)	0.00115 \pm 0.0004 (0.25s)	0.00217 \pm 0.0009 (95s)	0.00292 \pm 0.0009 (32s)
OOD d, N	0.0538 \pm 0.027 (0.10s)	0.0175 \pm 0.008 (0.45s)	0.0222 \pm 0.007 (157s)	0.0248 \pm 0.006 (100s)

Table 12: OpenML posterior-predictive comparison using one fixed AFIN configuration: flow decoder, standard Gaussian prior, and SNIS with 4096 proposal samples. Metrics are averaged over 16 binary OpenML datasets. Accuracy gap is AFIN minus TabPFN in percentage points.

Method	Prior / correction	Mean acc. \uparrow	Mean NLL \downarrow	Mean AUC \uparrow	Acc. win/tie
AFIN Flow	Standard + SNIS	0.857	0.397	0.827	6/16
TabPFN public v2	–	0.863	0.294	0.887	–
Mean acc. gap	AFIN - TabPFN	–0.53 percentage points			

most challenging split; NUTS gives the most accurate estimates there, but at substantially higher wall-clock cost.

D.8 Posterior-predictive transfer on OpenML

As an additional posterior-predictive sanity check, we compare AFIN with TabPFN public v2 on 16 binary OpenML classification datasets. For every dataset, AFIN uses the same Bayesian logistic-regression model,

$$z \sim \mathcal{N}(0, I), \quad y_i \mid x_i, z \sim \text{Bernoulli}(\sigma(x_i^\top z)),$$

with an intercept included in x_i . Continuous features are standardized using the training split, categorical features are one-hot encoded, and all methods use the same stratified 70/30 train/test split. We use the same trained flow-decoder AFIN from our experiments, with the standard Gaussian prior above and SNIS correction using 4096 proposal samples; no OpenML fine-tuning, task-specific prior tuning, or model selection is performed.

Table 12 shows that TabPFN is stronger on average, especially in NLL and AUC. AFIN is nevertheless close in accuracy, reaching 0.857 mean accuracy versus 0.863 for TabPFN and matching or exceeding TabPFN on 6 of 16 datasets. This experiment is not meant to position AFIN as a discriminative tabular predictor, but to check whether its posterior samples remain useful for real-data prediction without retraining.

Table 13 lists the datasets and processed dimensions. Table 14 reports the per-dataset metrics.

D.9 Additional results

Synthetic posterior accuracy by difficulty. Figures 5 to 7 show difficulty-wise versions of the synthetic posterior-vs-time experiment in Figure 2. Each figure averages over the same 16 prior-likelihood combinations and three random seeds, but fixes the difficulty level. Across easy, medium, and hard settings, the Gaussian-decoder AFIN checkpoint provides a strong single-shot posterior, and AFIN+SNIS improves rapidly with a small additional sampling budget. The hard setting is the most challenging because it is high-dimensional and data-poor, but AFIN+SNIS remains competitive with much longer NUTS and FRVI runs.

SNIS refinement by difficulty. Figures 8 to 10 show difficulty-wise versions of the SNIS refinement experiment in Figure 3. Each figure averages over 16 prior-likelihood combinations and three seeds at a fixed difficulty level. Across all three regimes, AFIN+SNIS starts from a low-cost amortized proposal and improves rapidly with additional SNIS samples, while FRVI+SNIS requires substantial per-task optimization before producing a competitive proposal.

Additional UCI metrics. Figures 11 and 12 complement the UCI sliced Wasserstein-2 results in Figure 4 by reporting posterior mean and covariance errors. The same qualitative pattern holds: AFIN

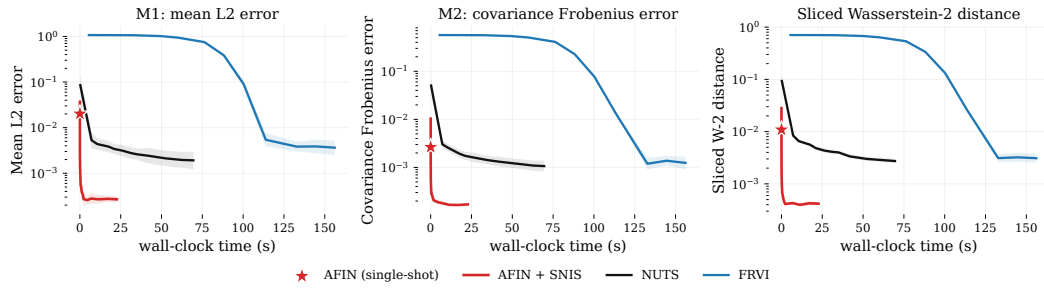


Figure 5: Synthetic posterior accuracy on easy tasks ($d = 4, N = 256$), averaged over 16 prior-likelihood combinations and three seeds. We use the Gaussian-decoder AFIN checkpoint. Points correspond to increasing test-time budgets: SNIS proposal samples for AFIN+SNIS, MCMC samples for NUTS, and optimization steps for FRVI. Posterior samples are compared with a long-run NUTS reference using mean L_2 error, covariance Frobenius error, and sliced Wasserstein-2 distance. Shaded bands show one standard deviation over seeds; lower is better.

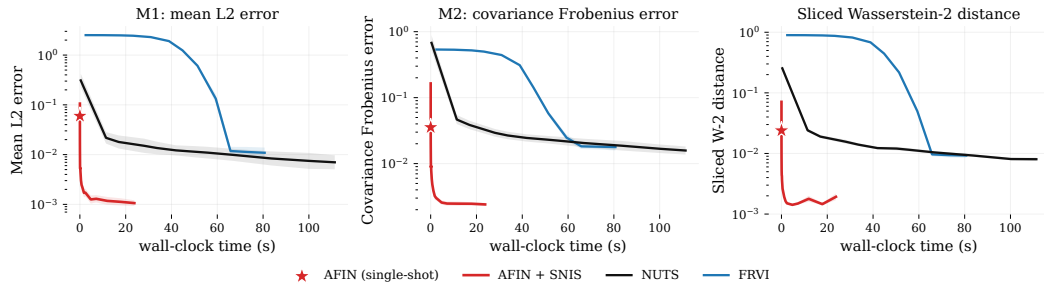


Figure 6: Synthetic posterior accuracy on medium tasks ($d = 8, N = 64$), averaged over 16 prior-likelihood combinations and three seeds. We use the Gaussian-decoder AFIN checkpoint. Points correspond to increasing test-time budgets: SNIS proposal samples for AFIN+SNIS, MCMC samples for NUTS, and optimization steps for FRVI. Posterior samples are compared with a long-run NUTS reference using mean L_2 error, covariance Frobenius error, and sliced Wasserstein-2 distance. Shaded bands show one standard deviation over seeds; lower is better.

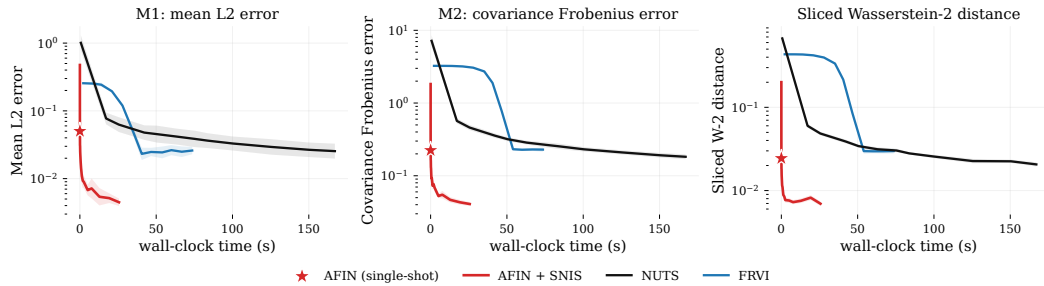


Figure 7: Synthetic posterior accuracy on hard tasks ($d = 16, N = 1$), averaged over 16 prior-likelihood combinations and three seeds. We use the Gaussian-decoder AFIN checkpoint. Points correspond to increasing test-time budgets: SNIS proposal samples for AFIN+SNIS, MCMC samples for NUTS, and optimization steps for FRVI. Posterior samples are compared with a long-run NUTS reference using mean L_2 error, covariance Frobenius error, and sliced Wasserstein-2 distance. Shaded bands show one standard deviation over seeds; lower is better.

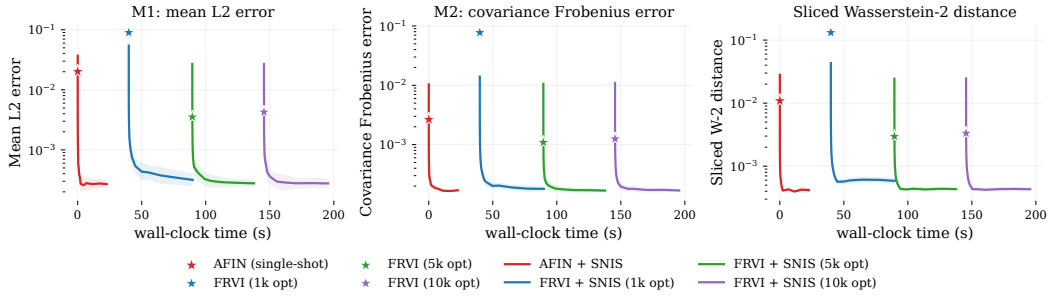


Figure 8: SNIS refinement on easy synthetic tasks ($d = 4, N = 256$), averaged over 16 prior-likelihood combinations and three seeds. AFIN+SNIS uses the Gaussian-decoder AFIN posterior as the proposal, while FRVI+SNIS uses FRVI proposals after 1k, 5k, or 10k optimization steps. Stars denote proposal quality before SNIS; curves vary the number of SNIS proposal samples. Metrics are computed against a long-run NUTS reference; lower is better.

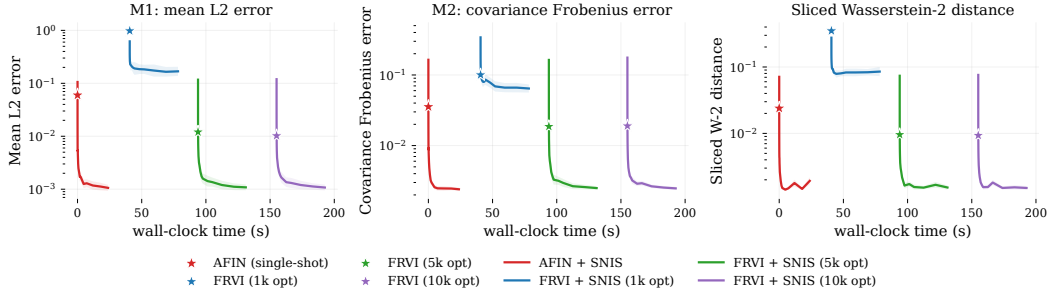


Figure 9: SNIS refinement on medium synthetic tasks ($d = 8, N = 64$), averaged over 16 prior-likelihood combinations and three seeds. AFIN+SNIS uses the Gaussian-decoder AFIN posterior as the proposal, while FRVI+SNIS uses FRVI proposals after 1k, 5k, or 10k optimization steps. Stars denote proposal quality before SNIS; curves vary the number of SNIS proposal samples. Metrics are computed against a long-run NUTS reference; lower is better.

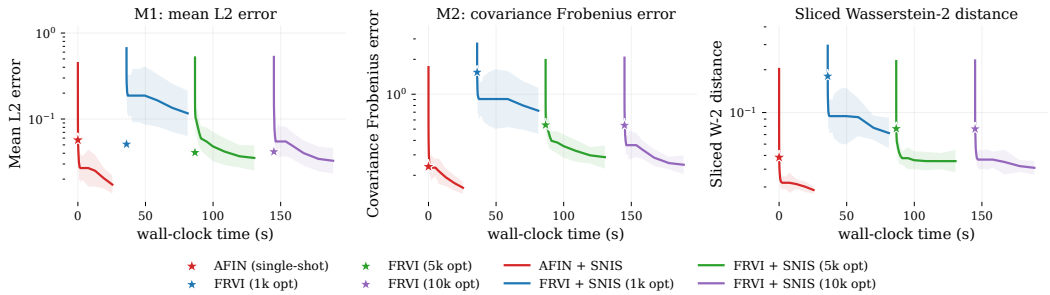


Figure 10: SNIS refinement on hard synthetic tasks ($d = 16, N = 1$), averaged over 16 prior-likelihood combinations and three seeds. AFIN+SNIS uses the Gaussian-decoder AFIN posterior as the proposal, while FRVI+SNIS uses FRVI proposals after 1k, 5k, or 10k optimization steps. Stars denote proposal quality before SNIS; curves vary the number of SNIS proposal samples. Metrics are computed against a long-run NUTS reference; lower is better.

Table 13: OpenML datasets used in the posterior-predictive comparison. N_{tr} and N_{te} denote train and test sizes. d_{feat} is the processed feature dimension before adding the intercept, and d_{model} is the latent dimension of the logistic-regression coefficient vector used by AFIN.

Dataset	OpenML ID	N_{tr}	N_{te}	d_{feat}	d_{model}
breast-w	15	478	205	9	10
credit-approval	29	457	196	46	47
credit-g	31	700	300	61	62
diabetes	37	537	231	8	9
haberman	43	214	92	14	15
heart-statlog	53	189	81	13	14
pc4	1049	1020	438	37	38
pc3	1050	1094	469	37	38
kc2	1063	365	157	21	22
pc1	1068	776	333	21	22
banknote-authentication	1462	960	412	4	5
blood-transfusion-service-center	1464	523	225	4	5
climate-model-simulation-crashes	1467	378	162	20	21
ilpd	1480	408	175	11	12
qsar-biodeg	1494	738	317	41	42
wdbc	1510	398	171	30	31

Table 14: Full OpenML posterior-predictive results. AFIN uses the fixed Flow + SNIS configuration from Table 12. Δ accuracy is AFIN minus TabPFN in percentage points.

Dataset	ID	Acc. AFIN	Acc. TabPFN	Δ acc.	NLL AFIN	NLL TabPFN	AUC AFIN	AUC TabPFN
breast-w	15	0.956	0.976	-2.0	0.102	0.098	0.995	0.994
credit-approval	29	0.888	0.888	0.0	0.316	0.271	0.933	0.955
credit-g	31	0.787	0.780	0.7	0.486	0.458	0.812	0.839
diabetes	37	0.784	0.766	1.7	0.438	0.432	0.868	0.866
haberman	43	0.761	0.750	1.1	0.570	0.500	0.609	0.753
heart-statlog	53	0.802	0.790	1.2	0.426	0.384	0.891	0.905
pc4	1049	0.890	0.902	-1.1	0.528	0.182	0.793	0.948
pc3	1050	0.889	0.896	-0.6	0.650	0.239	0.580	0.872
kc2	1063	0.841	0.866	-2.5	0.776	0.409	0.797	0.803
pc1	1068	0.925	0.940	-1.5	0.350	0.161	0.647	0.909
banknote-authentication	1462	0.988	1.000	-1.2	0.043	0.001	1.000	1.000
blood-transfusion-service-center	1464	0.764	0.787	-2.2	0.479	0.478	0.747	0.747
climate-model-simulation-crashes	1467	0.907	0.920	-1.2	0.196	0.184	0.932	0.929
ilpd	1480	0.714	0.720	-0.6	0.524	0.505	0.724	0.748
qsar-biodeg	1494	0.855	0.861	-0.6	0.367	0.301	0.913	0.939
wdbc	1510	0.965	0.959	0.6	0.107	0.099	0.992	0.992

provides a low-cost zero-shot posterior, AFIN+SNIS often improves it with a small additional sampling budget, and iterative baselines require substantially more wall-clock time to reach comparable accuracy.

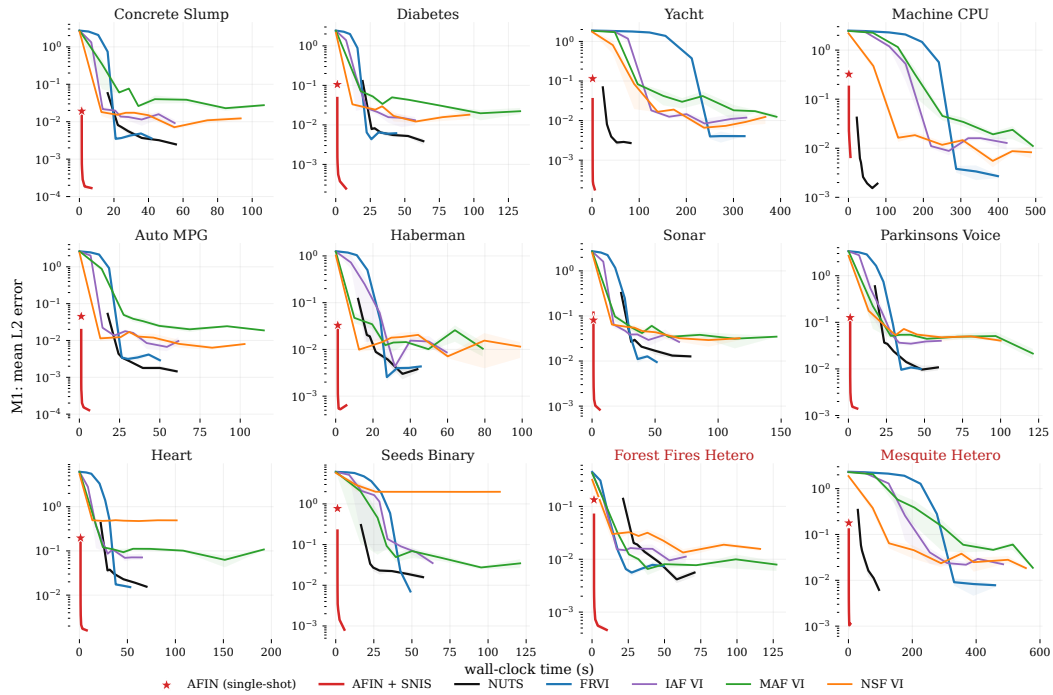


Figure 11: Zero-shot posterior mean accuracy on 12 UCI datasets using the Gaussian-decoder AFIN checkpoint. Each panel reports mean L_2 error to a long-run NUTS reference as a function of test-time wall-clock cost. Points correspond to increasing budgets: SNIS proposal samples for AFIN+SNIS, MCMC samples for NUTS, and optimization steps followed by posterior sampling for FRVI, IAF VI, MAF VI, and NSF VI. AFIN single-shot uses one network forward pass and no per-task optimization. Red titles indicate heterogeneous-likelihood tasks. Shaded bands show one standard deviation over three seeds; lower is better.

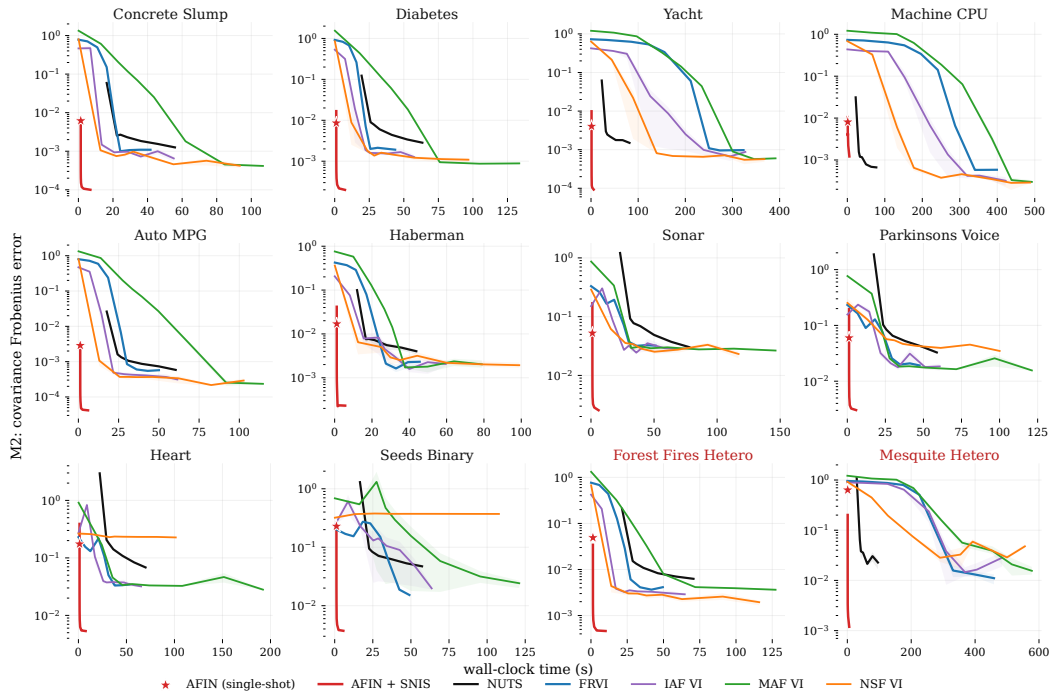


Figure 12: Zero-shot posterior covariance accuracy on 12 UCI datasets using the Gaussian-decoder AFIN checkpoint. Each panel reports covariance Frobenius error to a long-run NUTS reference as a function of test-time wall-clock cost. Points correspond to increasing budgets: SNIS proposal samples for AFIN+SNIS, MCMC samples for NUTS, and optimization steps followed by posterior sampling for FRVI, IAF VI, MAF VI, and NSF VI. AFIN single-shot uses one network forward pass and no per-task optimization. Red titles indicate heterogeneous-likelihood tasks. Shaded bands show one standard deviation over three seeds; lower is better.